Active Control of Flexible Structures using Fiber Optic Modal Domain Sensors

by

David Earl Cox

Thesis submitted to the Faculty of the
Virginia Polytechnic Institute and State University
in partial fulfillment of the requirements for the degree of
Master of Science
in
Electrical Engineering

APPROVED:

Douglas K. Lindner, Chairman

Richard O. Claus

William T. Baumann

May, 1990

Blacksburg, Virginia

Active Control of Flexible Structures

using

Fiber Optic Modal Domain Sensors

by

David Earl Cox

Douglas K. Lindner, Chairman

Electrical Engineering

(ABSTRACT)

The use of a modal domain fiber optic sensor for vibration control of a flexible cantilevered beam is experimentally demonstrated. The sensor utilizes mode-mode interference in a two mode elliptical core fiber. The sensor covers a major portion of the beam, and produces a measurement based on the strain distribution in the beam. A distributed-effect model is developed for the fiber optic sensor, and verified through both static and dynamic tests. This model is incorporated into a active control system employing dynamic output feedback. The control system is shown to add damping to the low order modes of the beam. Numerical simulations are presented which concur with the experimental responses, in both open and closed loop tests.

ACKNOWLEDGEMENTS

A great many people have devoted their time and energy towards the research described in this thesis. The most significant of these has been my advisor Dr. D. K. Lindner. Over the last two years his dedication and insight has helped me to turn ideas into projects, and speculations into facts. I have also had the pleasure of working with Dr. Richard Claus, director of the Fiber & Electro-Optics Research Center. His creative and open minded approach to research inspired many of my ideas. I also wish to thank Dr. W. T. Baumann. It was his enthusiastic teaching which sparked my interest in control theory, and in turn my interest in graduate school.

Although my committee has been invaluable, I must extend the greatest thanks to my parents. My education would not have been possible without their love and support. I wish to dedicate this work in memory of my mother, Mrs. Patricia R. Coyle. It was from her I drew the confidence to attempt, and the strength to succeed.

TABLE OF CONTENTS

LIST OF ILLUSTRATIONS

LIST OF TABLES

LIST OF SYMBOLS

Roman:

a - radius of fiber's core

A - state space system matrix

$A_{\nu m}$- complex amplitude constants

b - normalized propagation constant

B - state space input matrix

C - state space output matrix

d_{31}- charge constant of piezoelectric

D - damping matrix

E_b - Young's modulus of beam

E_p - Young's modulus of piezoelectric

E - complex electric field vector

f^-, f^+- end points of optical fiber

f_e - spatial dependence of electric field

f_h - spatial dependence of magnetic field

G - system transfer function

h_b- height of beam

h_p- height of piezoelectric

H - compensator transfer function

H - complex magnetic field vector

I - identity matrix

I_f - intensity pattern in optical fiber

I_m - moment of inertia about bending axis of beam

I_o - maximum nonlinear fiber signal

J_ν - Bessel function of first kind, order ν

K_ν - modified Bessel function of first kind, order ν

k_o - free space wave number

K - stiffness matrix

K_p - added stiffness from piezoelectric

LP - linearly polarized mode

M - mass matrix

m - linearly polarized mode index

n_1- index of refraction in fiber's core

n_2- index of refraction in fiber's cladding

l - length of beam

N - number of modes considered in the model

p^-, p^+- end points of piezoelectric patch

p_{11}, p_{12} - photoelastic constants

P - force applied at the beam's tip

Q - modal force vector

S_z - Poynting vector

t_b - thickness of beam

t_p - thickness of piezoelectric

U, W - waveguide parameters

v - voltage applied to piezoelectric

V - normalized frequency

x - state variable

y - displacement of beam from equilibrium

y_{md} - output of the modal domain sensor

z_o - gage length of fiber

z_f - strained length of the fiber

Greek:

β - propagation constant

$\Delta\beta$ - propagation difference between modes

$\Delta\tilde{\beta}$ - fringe frequency

δ_{nm} - Kronecker delta function

ϵ - strain along axis of fiber

ε - electric permittivity

$\mathfrak{E}$ - instantaneous electric field

$\mathfrak{H}$ - instantaneous magnetic field

Γ - phase difference between modes

ρ_l - linear density of beam (mass/unit length)

Λ_n - characteristic value for vibration eigenvalue problem

ψ_n - mode shapes

η_n - modal amplitudes

λ - optical wavelength

μ - magnetic permeability

ν - azimuthal mode index

υ - Poisson's ratio

ω - optical frequency

ς - damping factor

Operators: $\dot{x}$ - time derivative of x

x'- space derivative of x

x^* - complex conjugate of x

$\tilde{x}$ - approximate or perturbed value of x

$\hat{x}$ - x is a unit vector

∇^2 - Laplacian operator

1.0 INTRODUCTION

Many future aerospace projects will require the use of active systems to sense and control structural displacements. Large space platforms, such as the proposed space station, will be constructed from lightweight materials and assembled, at least in part, in space. Disturbances, such as the docking of spacecraft or firing of reboost rockets, will excite structural vibrations. Once excited these vibrations will continue with very little natural damping. An active control system could be used to protect the integrity of the structure, and improve operating conditions for space based equipment. This control system must utilize sensors to detect the vibrations, and actuators to apply forces which will counteract the effect of disturbances.

The control of large flexible structures is an active area of research. Some of this research has concentrated on the use of distributed-effect sensors and actuators. Distributed-effect sensors provide a scalar signal which is based on a distributed measurement, whereas distributed-effect actuators create a distributed force based on a scalar signal. Most of this work has utilized the distributed-effect properties of piezoelectric materials [1,2,3]. However, fiber optic sensors also have

the capability to make distributed-effect measurements. These sensors have other properties which make them advantageous in certain applications. The fiber optic sensor consists of a very small single strand of glass. It can be embedded in, or attached to a structure, with minimal loading. Fiber optic sensors have an extremely high bandwidth, and can be used to detect vibrations over a wide range of frequencies. Signals from fiber optic sensors neither contribute to, nor respond to electromagnetic noise. This property becomes important in systems with dense electronic equipment, or when electromagnetic shielding is difficult.

The goal of this research was to incorporate a fiber optic sensor into a closed loop control system for vibration suppression in a flexible structure [4,5]. To do this a distributed-effect system model was developed for the sensor, and verified through dynamic and static testing. The plant chosen to be controlled was a flexible cantilevered beam. The experimental arrangement is shown in Figure 1. Under disturbances the beam would exhibit one dimensional vibrations which decayed very slowly. A fiber optic sensor was mounted along the full length of the beam. Vibrations in the beam caused strain to be transferred to the fiber. The fiber's signal was a distributed-effect measurement of the strain distribution in the beam. A piezoelectric actuator was also mounted on the beam. The actuator allowed shear forces to be applied to a section of the beam. A digital feedback system was designed which derived control signals from the sensor, and applied them to the actuator.

The control system was designed to add damping to the beam so vibrations would decay more quickly. Since there were no concrete performance objectives a simple procedure was chosen for the design of the control law. The dynamics of

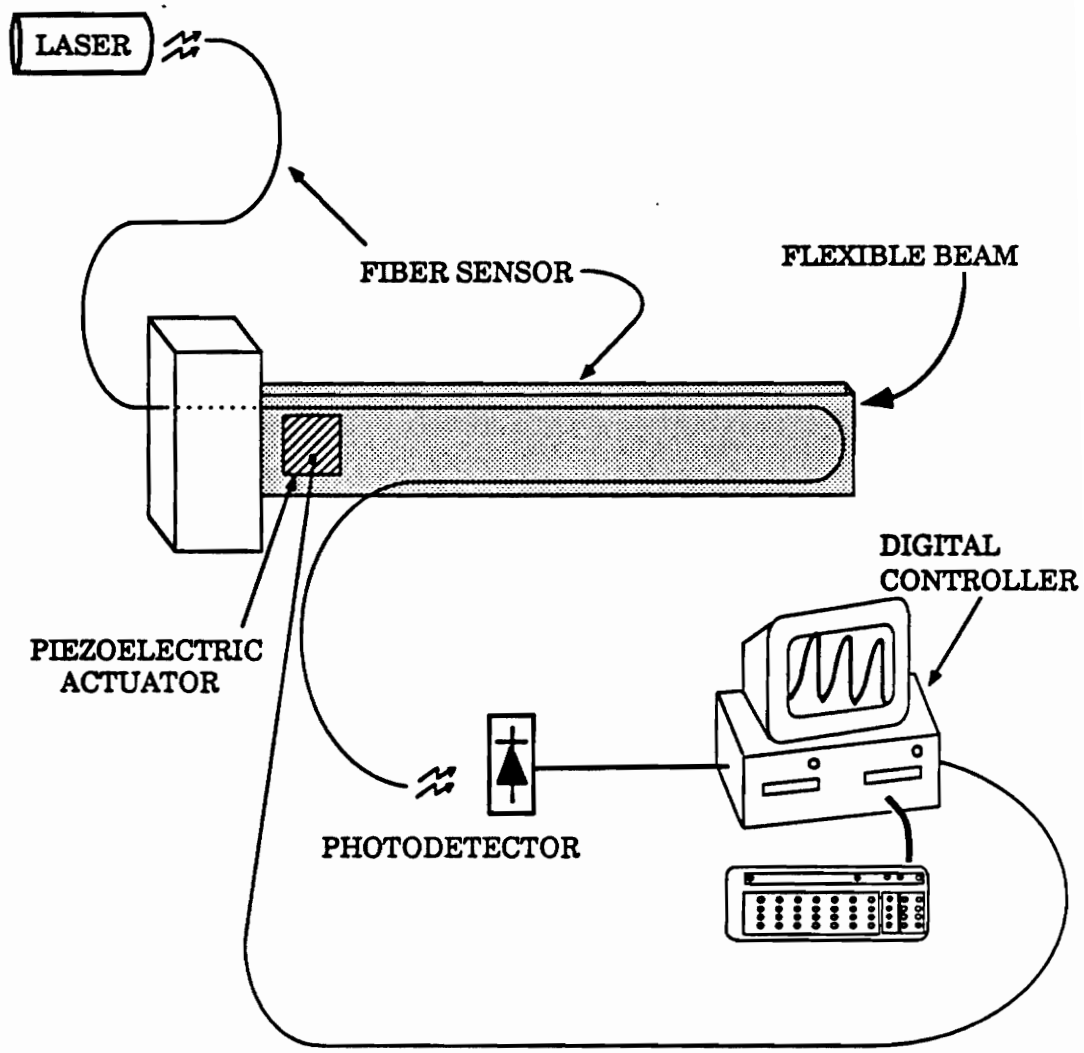

Figure 1. Overview of Experiment

the instrumented beam were carefully modeled, and simulation routines were used to predict the system's performance. Since the fiber optic sensor was the only novel component in the system, simulations could be used to verify the sensor's model. The simulated response was compared to the experimental response under a variety of conditions. The sensor model was found to behave as predicted in both open and closed loop configurations. This verified the sensor model, and demonstrated the ability to implement active control systems with fiber optic sensors.

Much research has been done in characterizing different types of fiber optic sensors [6,7]. The type chosen for this work was the modal domain sensor. Modal domain sensors utilize interference between the low order modes in a fiber to sense small changes in the fiber's length. Unlike a traditional interferometer no reference arm is required. This helps to stabilize the sensor and makes mounting it to structures more practical. This type of sensor was first described by Layton and Bucaro [8] in the late seventies. They applied the modal domain sensor to the detection of underwater acoustic waves. Since that time many others have studied the properties of few mode fibers. The coupling of power between the modes of few mode fibers has been described, and the construction of mode selective filters has been demonstrated [9,10]. The use of few mode fibers to measure static and dynamic strain distributions has been investigated in detail. The results of this research are documented in [11,12,13].

A significant improvement in modal domain sensing came with the introduction of elliptical core fibers. To characterize a modal domain sensor requires equations which describe the distribution of power in the fiber. Circular

core fibers support modes which are spatially degenerate. This degeneracy results in a spatial power distribution which depends upon the launch conditions of the incident light. In practice launch conditions are difficult to define or maintain. Therefore, consistent modeling of circular core modal domain sensors is difficult. Experimental evidence has shown that elliptical core fibers are not spatially degenerate [14,15]. This removes the dependance on launch conditions in the sensor's model, and allows for repeatable experiments.

The second chapter of this thesis develops a model for the modal domain sensor. The concept of modes in optical waveguides is defined. The spatial interference pattern in a two mode fiber is derived, and shown to vary under the influence of strain. In Chapter 3 the equations which describe the dynamic behavior of the flexible beam are given. The model for the modal domain sensor is incorporated into a state space representation for the system. Chapter 4 describes the design of the experiment and the development of a dynamic compensator. All physical parameters associated with the system are listed. Details of the optical hardware used to construct the modal domain sensor are also given. The results from simulation and experiment are given in Chapter 5. A series of tests are performed to verify the beam dynamics, actuator model, and sensor model independently. To test the interaction of these components experiments are presented which detail the open and closed loop system behavior. Chapter 6 presents some conclusions, and outlines areas of interest for future work.

2.0 MODAL DOMAIN SENSORS

This chapter develops the theory for fiber optic modal domain sensors. The first section gives an introduction into fiber optics and establishes some terminology. Section 2.2 defines the electromagnetics problem associated with optical waveguides. The equations describing linearly polarized modes in a circular core fiber are presented. In Section 2.3, the modal domain sensor is described as a fiber which supports only two modes. The distribution of power in the fiber is shown to be a function of axial distance. The sensor's response to strain is discussed in Section 2.4. A model for the modal domain sensor is developed. This is the model used to incorporate the sensor into a dynamic control system. Section 2.5 discusses the practical advantages of elliptical core fibers.

2.1 OPTICAL FIBERS

Optical fibers are cylindrical dielectrics which act as waveguides for light. Typically they are drawn from extremely pure glass. An optical fiber has two concentric regions. The central region, called the core, is surrounded by a region

called the cladding. These regions are both glass, but have different indices of refraction. The index of refraction of the core, n_1, must be greater than the cladding index, n_2. However, for the fibers of interest here the index difference is very small, $\frac{n_1}{n_2} \approx 1$. When the core index is constant, but changes discontinuously at the cladding boundary, the fiber is called a step index fiber. Other index profiles exist which will guide light, but they will not be discussed in this thesis. Fibers are usually covered with a plastic jacket. The jacket forms a protective conduit for the waveguide, providing flexibility to the otherwise brittle glass. Since the jacket does not affect the waveguide properties, it will not be considered in the analysis of the modal domain sensor.

The transmission of light in a fiber can be conceptually explained using ray optics. The core-cladding index difference allows total internal reflection to occur within the fiber. Light rays which strike the core-cladding boundary are split into reflected and refracted rays. Since the cladding index is less than the core index the angle which the refracted ray makes with the boundary is less than the angle of the incident ray. When the angle of incidence reaches the critical angle the refracted ray is directed along the core-cladding boundary. Refraction cannot occur for rays incident at angles below the critical angle, and these light rays remain with the fiber's core. Figure 2 shows a light ray reflected down a step index fiber. Although ray theory is a useful tool it is only valid if the core radius is large compared to the wavelength of light. This is not the case with optical fibers. To obtain an accurate description of the light in an optical fiber requires the concept of optical modes. The definition and form of these modes is the topic Section 2.2.

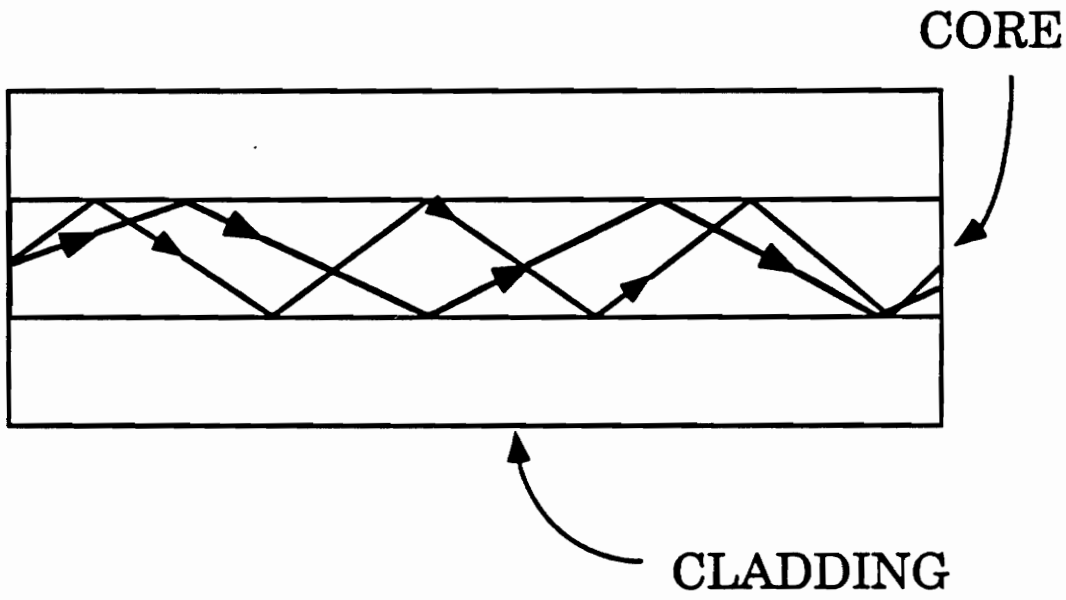

Figure 2. Light rays in a step index fiber

Optical fibers are classified into two categories; multimode fibers, and single mode fibers, depending on their commercial use. The distinction between the two is determined by the number of modes, the fiber will support. Single mode fibers will only support one mode, while multimode fibers typically support hundreds of modes. The number of modes an optical fiber will support is determined by the fiber parameters and the wavelength of the source. Therefore, when a fiber is referred to as single mode it implies operation at a certain source wavelength. The reference 633 nm single mode fiber, describes a fiber which supports only one mode at a wavelength of 633 nm. At a shorter wavelength the fiber may support two, three, or more modes. Although this operation is technically multimode, it is referred to as a few mode fiber. The main physical difference between single mode fibers and multimode fibers, is in the core size. Multimode fibers usually have a core radius of about 25 μm, while single mode fibers have a core radius of about 4μm. Both types of fibers are drawn with claddings which extend to 62.5μm. This cladding is sufficiently thick that the cladding-jacket interface can be ignored in the waveguide analysis.

Light in an optical fiber is not uniformly distributed in the cross section of the core. In single mode fibers the intensity is brightest in the center of the core, and dimmest near the cladding interface. In few mode fibers a predictable intensity pattern is formed by interference between the modes. This interference creates an intensity pattern that varies both in cross section, and along the length of the fiber. It is the length variation which is utilized in modal domain sensing. The modal domain sensor described here has only two modes propagating in the fiber. A two mode fiber is obtained by operating a single mode fiber at a wavelength below its specified frequency range.

2.2 OPTICAL MODES

Light is described by the propagation of harmonically varying electric and magnetic fields. In general these fields can be written,

$$\mathcal{E}(\vec{r},t) = \mathcal{R}e\left[f_e(\vec{r})\, e^{j\vec{\beta}\cdot\vec{r}} e^{j\omega t}\right]\hat{a}_e, \tag{2.2.1}$$

$$\mathcal{H}(\vec{r},t) = \mathcal{R}e\left[f_h(\vec{r}) e^{j\vec{\beta}\cdot\vec{r}} e^{j\omega t}\right]\hat{a}_h, \tag{2.2.2}$$

where

$\mathcal{E}$ = real electric field vector,
$\mathcal{H}$ = real magnetic field vector,
f_e = spatial dependence of electric field,
f_h = spatial dependence of magnetic field,
$\vec{\beta}$ = propagation vector,
$\vec{r}$ = three dimensional spatial vector,
ω = frequency of the optical source,
$\hat{a}_e$ = unit vector in direction of electric field, and
$\hat{a}_h$ = unit vector in direction of magnetic field.

The analysis in this section develops a description for the electromagnetic fields inside an optical fiber. The source is assumed to produce monochromatic polarized light. Polarized light has the property that the electric field does not rotate in space, i.e. $\hat{a}_e$ is a constant. The spatial dependance of the fields will be described using the cylindrical coordinate system shown in Figure 3. The vector properties of the field, however, will be described using cartesian unit vectors. The z axis of both the cartesian and cylindrical coordinate systems are aligned

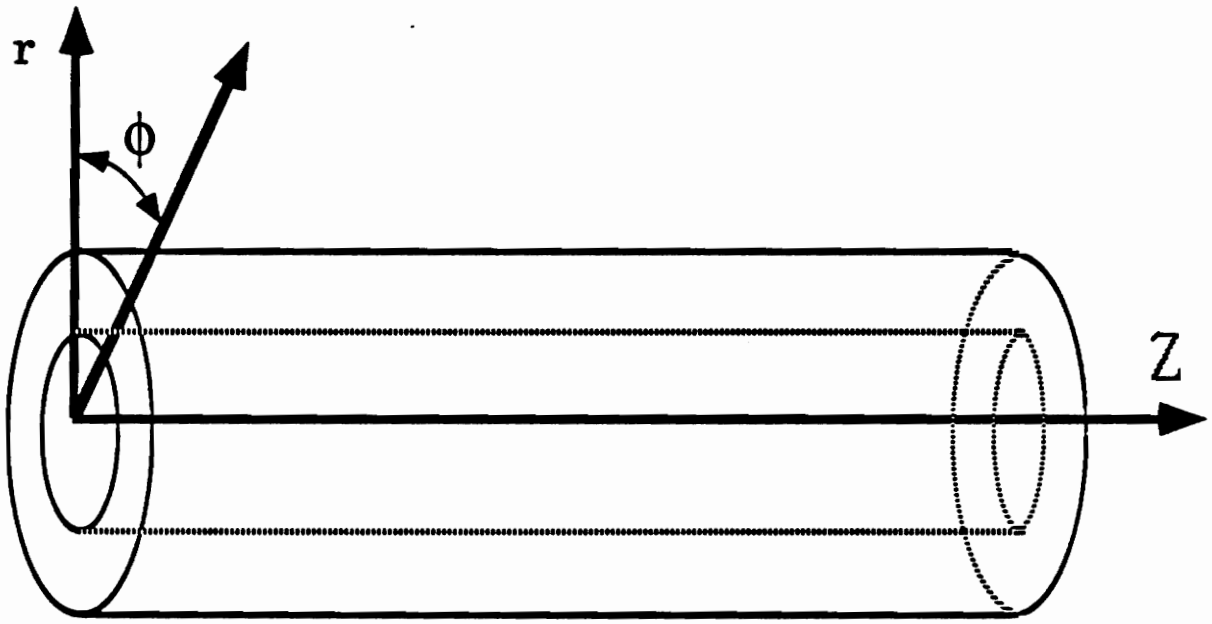

Figure 3. Cylindrical coordinate system in optical fiber

with the axis of the fiber. Complex phasor representations will be used to describe the electric and magnetic fields. The real fields can be obtained from the complex field descriptions via,

$$\mathcal{E}(r,\phi,z,t) = \Re e\left[\mathbf{E}(r,\phi,z)e^{j\omega t}\right], \tag{2.2.3}$$

$$\mathcal{H}(r,\phi,z,t) = \Re e\left[\mathbf{H}(r,\phi,z)e^{j\omega t}\right], \tag{2.2.4}$$

where

$\mathbf{E}$ = complex electric field vector, and

$\mathbf{H}$ = complex magnetic field vector.

The complex field vectors can be written in terms of scalar field components and cartesian unit vectors,

$$\mathbf{E}(r,\phi,z) = E_x(r,\phi,z)\hat{x} + E_y(r,\phi,z)\hat{y} + E_z(r,\phi,z)\hat{z}, \tag{2.2.5}$$

$$\mathbf{H}(r,\phi,z) = H_x(r,\phi,z)\hat{x} + H_y(r,\phi,z)\hat{y} + E_z(r,\phi,z)\hat{z}. \tag{2.2.6}$$

A full description of the electromagnetic waves in an optical fiber is given by solving Maxwell's equations under the appropriate boundary conditions. In the case of optical fibers the constraints imposed by Maxwell's equations can be expressed in the form of two vector wave equations,

$$\nabla^2\mathbf{E} + \omega^2\mu\varepsilon\mathbf{E} = 0, \tag{2.2.7}$$

$$\nabla^2\mathbf{H} + \omega^2\mu\varepsilon\mathbf{H} = 0, \tag{2.2.8}$$

where

∇^2 = Laplacian operator,

ε = electric permittivity, and

μ = magnetic permeability.

Since the magnetic and electric field vectors are governed by equations of the same form, only the electric field vector will be developed explicitly. We are looking for solutions to (2.2.7) which remain guided in the core region. Therefore, we assume the propagation vector to be in the z direction. The form which these guided solutions take is in general quite cumbersome, and a full derivation can be found in [16]. However, the solutions can be simplified by making the assumption that the core and cladding indices are nearly equal. Such fibers are termed weakly guiding fibers, and are of the type used for modal domain sensing. This assumption has been shown to remove E_z, the transverse field component [17]. The fields are then confined to the x-y plane, and solutions to the wave equation are linearly polarized.

The direction of the electric field in the x-y plane is determined by the polarization of the source. We can assume, without loss of generality, that the fields are polarized directly along the x axis. This removes the term E_y, and reduces (2.2.7) to a scalar wave equation. The form of the electric field vector for a weakly guided solution of the wave equations is,

$$\mathbf{E} = \begin{bmatrix} AJ_\nu(Ur)\begin{bmatrix}\cos(\nu\phi)\\ \sin(\nu\phi)\end{bmatrix} e^{-j\beta z}\,\hat{x} & \text{for } r<a \\ BK_\nu(Wr)\begin{bmatrix}\cos(\nu\phi)\\ \sin(\nu\phi)\end{bmatrix} e^{-j\beta z}\,\hat{x} & \text{for } r>a \end{bmatrix}, \tag{2.2.9}$$

where

$$U = \sqrt{k_o^2 n_1^2 - \beta^2},$$
$$W = \sqrt{\beta^2 - k_o^2 n_2^2},$$

$k_o = \omega_o\sqrt{\mu\varepsilon}$,
J_ν = Bessel function of the first kind, order ν,
K_ν = modified Bessel function of the first kind, order ν,
β = propagation constant, and
a = radius of the core.

The field solution must be periodic in ϕ, with a maximum period of 2π. This restricts ν to the set of integers. The $\begin{bmatrix}\cos(\nu\phi)\\ \sin(\nu\phi)\end{bmatrix}$ term in (2.2.9) expresses a degeneracy in the form of the solution. The final solution may have an azimuthal dependence on either sine or cosine, or a linear combination of both. The solution which has a cosine dependence is referred to as the even solution, and the solution which has a sine dependence is referred to as the odd solution.

The existence of these solutions is determined by the application of boundary conditions. The boundary conditions in a fiber require that the tangential components of the electric field vector and the magnetic field vector are continuous at the core-cladding interface. Application of these conditions forms the following eigenvalue problem,

$$\frac{J_\nu(Ua)}{UJ_{\nu-1}(Ua)} + \frac{K_\nu(Wa)}{WK_{\nu-1}(Wa)} = 0. \qquad (2.2.10)$$

This is the waveguide characteristic equation. Solutions to this equation define the linearly polarized modes. For each integer ν, there are an infinite number of solutions to (2.2.10). These solutions are typically labeled $LP_{\nu m}$, where m refers to the mth solution of (2.2.10). The double subscript, (νm), will be used to designate propagation constants, electric field vectors, and other parameters corresponding to a particular LP mode. The modes which can actually be excited

in a fiber are determined by the source frequency, and launch conditions. At a single source frequency only a finite number of modes can exist within the fiber. It is possible, with a monochromatic source of the appropriate frequency, to have only two modes supported by the fiber. This is the type of source-waveguide system which is used for modal domain sensing.

Dispersion curves generalize the solutions of the characteristic equation to the entire class of step index, circular core fibers. This is accomplished by parameterizing the solutions by the normalized frequency, and the normalized propagation constant. The normalized frequency is defined,

$$V = k_o a \sqrt{n_1^2 - n_2^2}, \tag{2.2.11}$$

and the normalized propagation constant is defined,

$$b_{\nu m} = \frac{(\beta_{\nu m}/k_o)^2 - n_2^2}{n_1^2 - n_2^2}. \tag{2.2.12}$$

The dispersion curves are shown in Figure 4. Each curve is labeled with its linearly polarized mode index (νm). It is apparent from these curves that if the normalized frequency is between 2.41 and 3.83 only the LP_{01} and LP_{11} modes are supported by the waveguide. This range of normalized frequency can be obtained by choosing the appropriate radius, indices of refraction, and source wavelength. The interference pattern in a two mode fiber has a relatively simple description, which is developed in the next section.

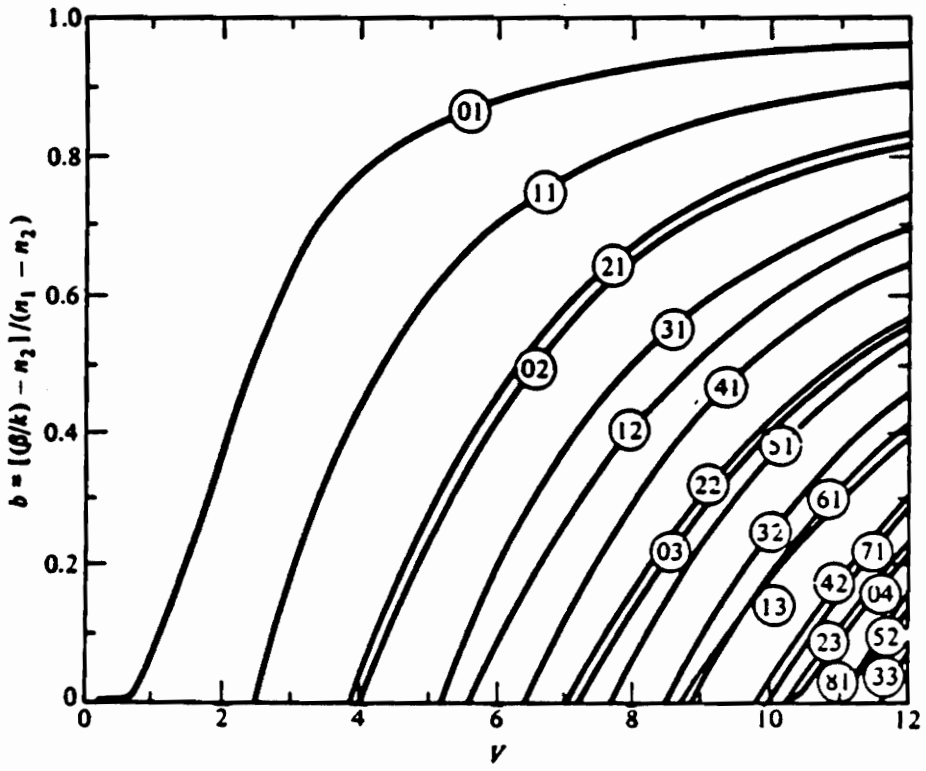

Figure 4. Dispersion curves

2.3 INTERFERENCE PATTERNS

The distribution of power in the cross-section of a fiber is given by the Poynting vector. This vector is defined,

$$S_z = \frac{1}{2}\Re e[\mathbf{E} \times \mathbf{H}^*]\cdot\hat{z}. \tag{2.3.1}$$

Under the assumption of linearly polarized modes **E** and **H** remain orthogonal to each other, as well as to the z axis. Since the fiber has a homogeneous characteristic impedance, the magnetic field vector is proportional to the electric field vector. Therefore, the distribution of power is proportional to the magnitude squared of the electric field vector. In a dual mode fiber this intensity is given by,

$$I_f(r,\phi,z) = \left|\mathbf{E}_{01}(r,\phi,z) + \mathbf{E}_{11}(r,\phi,z)\right|^2. \tag{2.3.2}$$

Most of the power in an optical fiber is confined to the core region. Therefore, this analysis will only develop the intensity distribution in the fiber's core. From (2.2.9) we have the electric field vector for the LP_{01} mode is

$$\mathbf{E}_{01}(r,\phi,z) = A_{01}J_0(U_{01}r)e^{-j\beta_{01}z}\,\hat{x}, \tag{2.3.3}$$

and the electric field vector for the LP_{11} mode is

$$\mathbf{E}_{11}(r,\phi,z) = \{A_{11}^e\cos(\phi) + A_{11}^o\sin(\phi)\}\,J_1(U_{11}r)e^{-j\beta_{11}z}\,\hat{x}, \tag{2.3.4}$$

where A_{11}^e and A_{11}^o are the amplitude constants for even and odd components, respectively. Launch conditions describe the distribution and polarization of light at the input end of the fiber. It is possible to adjust the launch conditions such

that only one degenerate component of the LP_{11} mode is excited [18]. Assume that the launch conditions are such that $A_{01}=A_{11}^{e}=1$, and $A_{11}^{o}=0$. This corresponds to the LP_{01} and LP_{11} even modes being excited in phase with equal amplitude, while the LP_{11} odd mode is not excited. The intensity distribution defined by (2.3.2) becomes,

$$I_f(r,\phi,z)=J_0^2(U_{01}r) + J_1^2(U_{11}r)\cos^2(\phi) + 2J_0(U_{01}r)J_1(U_{11}r)\cos(\phi)\cos(\Delta\beta z), \quad (2.3.5)$$

where $\Delta\beta = \beta_{01}$-β_{11}. This intensity pattern is shown in Figure 5, as a function of r and ϕ, for a fixed value of z. The important property of (2.3.5) is that the intensity pattern in the cross section of the fiber varies as $\cos(\Delta\beta z)$. The term $\Delta\beta z$ represents the phase difference between the modes. Since this phase difference varies with z, the intensity will undergo constructive and destructive interference along the fiber.

2.4 STRAIN RESPONSE

This section derives a model for the modal domain sensor by determining the effect of strain on the intensity pattern. The intensity pattern is assumed to be monitored at the end face of the fiber, denoted z_f. The strain is assumed to be applied exclusively along the axis of the fiber. Axial strain causes three major effects. The first two are concerned with the dimensions of the fiber. Under strain the fiber's length and radius will change. The third factor is a change in the index of refraction of the core and cladding.

The length of a fiber under strain is given by,

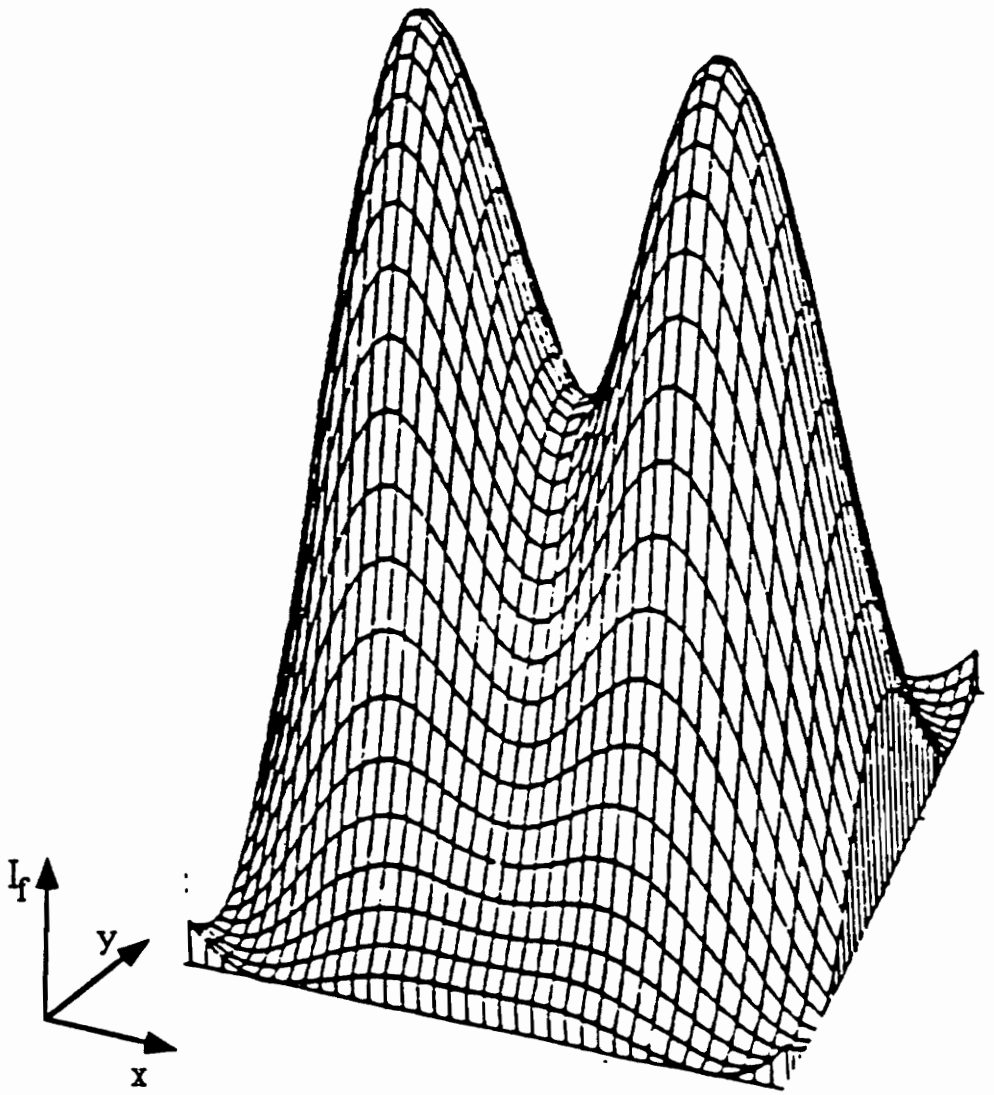

Figure 5. Three dimensional view of intensity pattern

$$z_f = z_o + \int_0^{z_o} \epsilon(z)dz, \tag{2.4.1}$$

where

z_o = unstrained fiber length, and

$\epsilon(z)$ = axial strain distribution.

The change in radius is due to the Poisson effect. The fiber's radius becomes a function of the axial strain distribution,

$$a(z) = a - \upsilon a\epsilon(z), \tag{2.4.2}$$

where υ is Poisson's ratio. The relationship between index of refraction and strain is given by the photoelastic effect [19],

$$n_i(z) = n_i - \frac{1}{2}n_i^3[(1-\upsilon)p_{12} - \upsilon p_{11}]\epsilon(z), \quad i=1,2 \tag{2.4.3}$$

where p_{11} and p_{12} are photoelastic constants. The photoelastic constants are standard material properties, and the subscript notation is not related to the linearly polarized mode indices.

The intensity pattern defined by (2.3.5) can be written,

$$I_f(r,\phi,z) = I_1(r,\phi) + I_2(r,\phi)\cos(\Gamma), \tag{2.4.4}$$

where the term Γ expresses the phase difference between the modes. Under zero strain this term was simply $\Delta\beta z$, however, in general we must define the phase difference as,

$$\Gamma = \int_0^z \Delta\beta(z)dz. \tag{2.4.5}$$

The effect refractive index and radius variations have on the intensity pattern is in general very complex. Standard treatment assumes I_1 and I_2 remain constant under strain, and considers only the change in the intermodal phase difference [13]. The change in radius and refractive indices will redefine the characteristic equation, and causes changes in $\Delta\beta$. This relationship can be written in terms of a Taylor series expansion. Ignoring higher order terms we have,

$$\Delta\beta(z) = \Delta\beta_o + \alpha\epsilon(z), \tag{2.4.6}$$

where $\Delta\beta_o$ is the propagation difference at zero strain. Substituting into (2.4.5) yields,

$$\Gamma = \int_0^z \left[\Delta\beta_o + \alpha\epsilon(z)\right] dz. \tag{2.4.7}$$

The phase difference at the end face of the fiber is,

$$\Gamma_f = \int_0^{z_o} \left[\Delta\beta_o + \alpha\epsilon(z)\right] dz + \int_{z_o}^{z_f} \Delta\beta_o dz. \tag{2.4.8}$$

This can be expressed,

$$\Gamma_f = \Delta\beta_o z_o + \Delta\tilde{\beta} \int_0^{z_o} \epsilon(z) dz, \tag{2.4.9}$$

where $\Delta\tilde{\beta} = (1+\alpha)\Delta\beta_o$. The intensity pattern as a function of strain can now be written,

$$I_f(\epsilon;r,\phi,z) = I_1(r,\phi) + I_2(r,\phi)\cos\left[\Delta\beta_o z_o + \Delta\tilde{\beta}\int\epsilon(z)dz\right]. \tag{2.4.10}$$

Strain is measured by monitoring this pattern at the end face of the fiber. Since there is no loss mechanism associated with modal interference the total power in the fiber's cross section must stay constant. Therefore, if the power in

the entire pattern is monitored no net change will be seen. Strain simply causes the power to be redistributed in the core. To obtain an amplitude modulated signal part of the core must be blocked by a spatial filter. Assume that exactly half of the core is blocked, and light from half the core strikes a photodetector. The signal from the photodetector is given by,

$$y_{md} = \int_0^a \int_{\frac{-\pi}{2}}^{\frac{\pi}{2}} I_1(r,\phi) + I_2(r,\phi)\cos\left[\Delta\beta_o z_o + \Delta\tilde{\beta}\int\epsilon(z)dz\right]d\phi dr. \qquad (2.4.11)$$

Since I_1 and I_2 depend only on r and ϕ, the integration causes these terms to be reduced to constants. The output of the sensor is then simply a raised sinusoid,

$$y_{md} = I_{DC} + I_o\cos\left[\Delta\beta_o z_o + \Delta\tilde{\beta}\int\epsilon(z)dz\right]. \qquad (2.4.12)$$

Figure 6 shows a graph of y_{md}. To achieve maximum sensitivity, as well as maximum linear operating range, the term $\Delta\beta_o z_o$ should be a multiple of $\frac{3\pi}{2}$. This corresponds to the two modes being 270° out of phase at the fiber's end face. This condition is referred to as the quadrature point, or Q-point. To achieve the Q-point the fiber must have a specific gage length. In practice this gage length is obtained by statically prestraining the fiber. It is also desirable to have the sensor's signal be zero at quadrature. Detection electronics are utilized to remove the signal's DC offset. The detected signal is then,

$$y_{md} = I_o\sin\left[\Delta\tilde{\beta}\int_0^{z_0}\epsilon(z,t)\ dz\right]. \qquad (2.4.13)$$

The signal will oscillate through an entire cycle with a fiber elongation of $\frac{2\pi}{\Delta\tilde{\beta}}$.

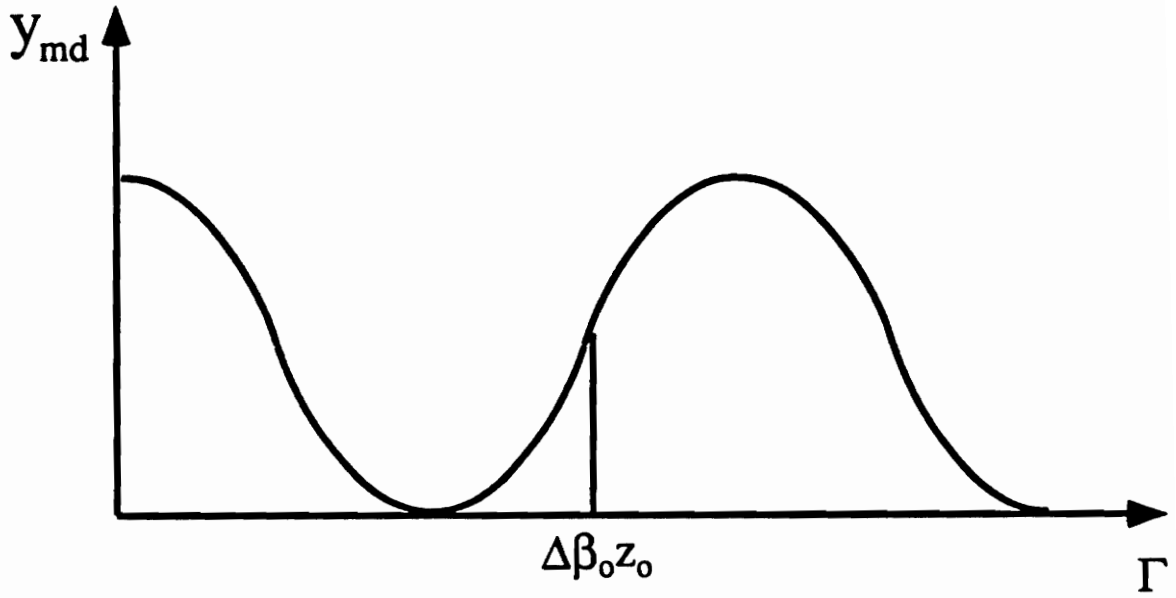

$$y_{md} = I_{DC} + I_o \cos\left\{ \Delta\beta_o z_o + \Delta\tilde{\beta} \int \varepsilon(z) dz \right\}$$

Figure 6. Modal domain sensor's dependence on strain

These cycles are known as fringes, since they are analogous to the spatial fringe patterns seen with traditional interferometers. We will refer to $\Delta\tilde{\beta}$ as the fringe frequency, and $\frac{2\pi}{\Delta\tilde{\beta}}$ as the fringe length of the sensor. For strain distributions which are small compared to the fringe length the sine term in (2.4.13) can be linearly approximated, and the sensor will produce a signal proportional to integral strain,

$$\tilde{y}_{md} = I_o \Delta\tilde{\beta} \int_0^{z_0} \epsilon(z,t)\, dz. \qquad (2.4.14)$$

This equation forms the linear model which describes the modal domain sensor's response to applied strain. The signal is directly proportional to the fiber's change in length. Therefore, it can be calibrated to units of distance. The remainder of this thesis discusses the use of this measurement in a classical control system.

2.5 ELLIPTICAL CORE FIBERS

In the analysis above it was assumed that the LP_{11} even mode was excited while the LP_{11} odd mode was not. Although it is possible to adjust launch conditions such that this is the case, maintaining these conditions is difficult in practice. Furthermore, it is difficult to keep power from coupling between the modes when the fiber is strained. Power which is coupled into the LP_{11} odd mode will cause the intensity distribution in the core to change. Since the mechanics of this coupling are difficult to define, the resulting signal does not vary predictably under strain. Circular core modal domain sensors, therefore, are not robust and are difficult to work with in practice.

It has been shown, experimentally, that elliptical core fibers do not exhibit spatially degenerate patterns in the second mode [14,15]. The elliptical core mode which corresponds to LP_{11} odd has a higher cutoff frequency than does the mode corresponding to LP_{11} even. This means that there exists a significant frequency range for which the LP_{11} even mode remains guided while the LP_{11} odd mode does not. Operating the modal domain sensor in this region prevents modal coupling, and eliminates the need for specific launch conditions.

Elliptical core fibers also do not exhibit a polarization degeneracy. The propagation constant of a mode depends upon the direction of polarization. Such fibers are referred to as being birefringent. The propagation of a mode in an elliptical core fiber must be decomposed into fields along the minor and major axis of the ellipse. The model for the elliptical core sensor will depend upon the polarization of the source, and orientation of the ellipse. To remain consistent with the circular core model light must be launched polarized directly along the major or minor axis of the elliptical core fiber.

Although the analysis given in this chapter does not apply directly to elliptical core fibers, the concept of dual mode interference remains the same. Elliptical core modes are assumed to be a perturbation of their circular core counterparts. The significant differences are not in the analytic form, but rather in the conditions required to excite the modes. The complete description for the modes of an elliptical core fiber is an area of current research. Approximate solutions have been found, and are reported in [20,21,22]. Due to the practical advantages, elliptical core fibers were utilized for the modal domain sensing experiments described in this thesis. The source polarization was adjusted so as

to minimize the effects of birefringence. Within a linear range of operation the circular core model proved to be an adequate description of the sensor's behavior.

3.0 SYSTEM MODEL

This chapter describes the construction of a linear state space model for a cantilevered flexible beam. A patch of piezoelectric material is mounted near the root of the beam, and is used as an actuator. A modal domain sensor is bonded along the beam's length, and is used as a sensor. The system discussed is shown in Figure 7. Section 3.1 develops the system dynamics under the assumptions of a Bernoulli-Euler beam model. Separation of variables is applied to form a solution, and the orthogonality of mode shapes is used to establish independent dynamics for each mode. The modal domain sensor is incorporated into the system model in Section 3.2. In Section 3.3 the use of piezoelectric actuators is described. The actuators are assumed to impart negligible mass loading, and drive the system through the application of shear forces.

3.1 BEAM DYNAMICS

If a beam's length is large compared to its height, and its height is large compared to its width, vibrations will occur primarily in one dimension. If these vibrations are small, the beam's mid-surface will experience no strain, and a

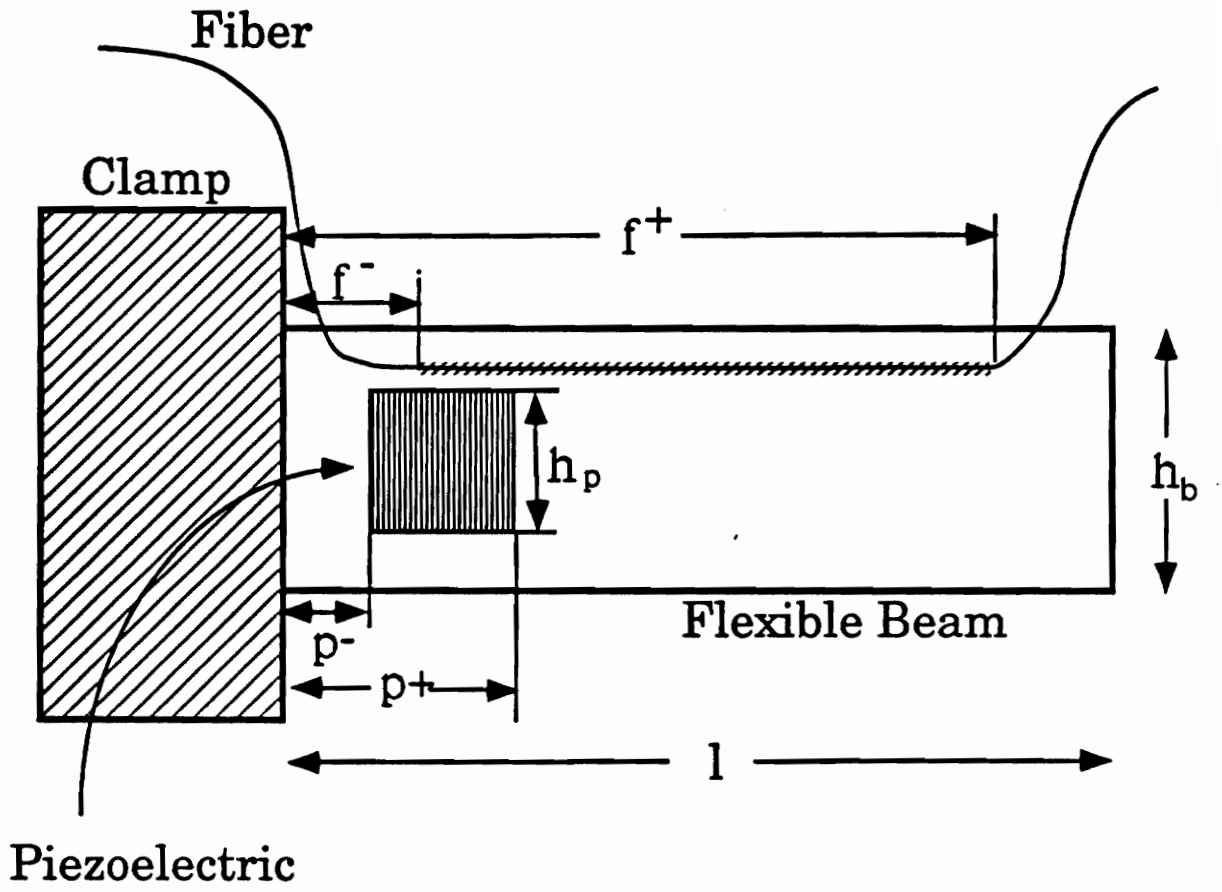

Figure 7. Instrumentation of flexible beam

Bernoulli-Euler description can be applied [23]. The two dimensional coordinate system used in this chapter is shown in Figure 8. The Bernoulli-Euler differential equation which describes the free vibration of a beam is

$$\frac{\partial^2}{\partial z^2}\left[E_b I_m(z)\frac{\partial^2}{\partial z^2}y(z,t)\right] + \rho_l(z)\frac{\partial^2}{\partial t^2}y(z,t)=Q(t), \qquad (3.1.1)$$

where

$y(t,z)$ = displacement function,

$Q(t)$ = modal forcing function,

$I_m(z)$= moment of inertia about the beam's bending axis,

$\rho_l(z)$ = linear density of the beam, and

E_b = Young's modulus of the beam's material.

Although the inertia and density may vary with length, the development here assumes a uniform beam. A more general treatment of the Bernoulli-Euler equation can be found in [24]. The boundary conditions for this equation are derived from physical observations. The beam's displacement must be zero at the clamped end. The beam's displacement must remain zero through the clamp. Therefore, the slope of the displacement must also be zero at the clamped end. Since the beam's free end can experience no reaction forces, the stress and shear at this point must be zero. Stress and shear are proportional to the second and third derivatives of displacement, respectively. These conditions are summarized,

$$y(0,t)=\frac{\partial}{\partial z}y(0,t)=\frac{\partial^2}{\partial z^2}y(l,t)=\frac{\partial^3}{\partial z^3}y(l,t)=0, \qquad (3.1.2)$$

where l is the beam's length.

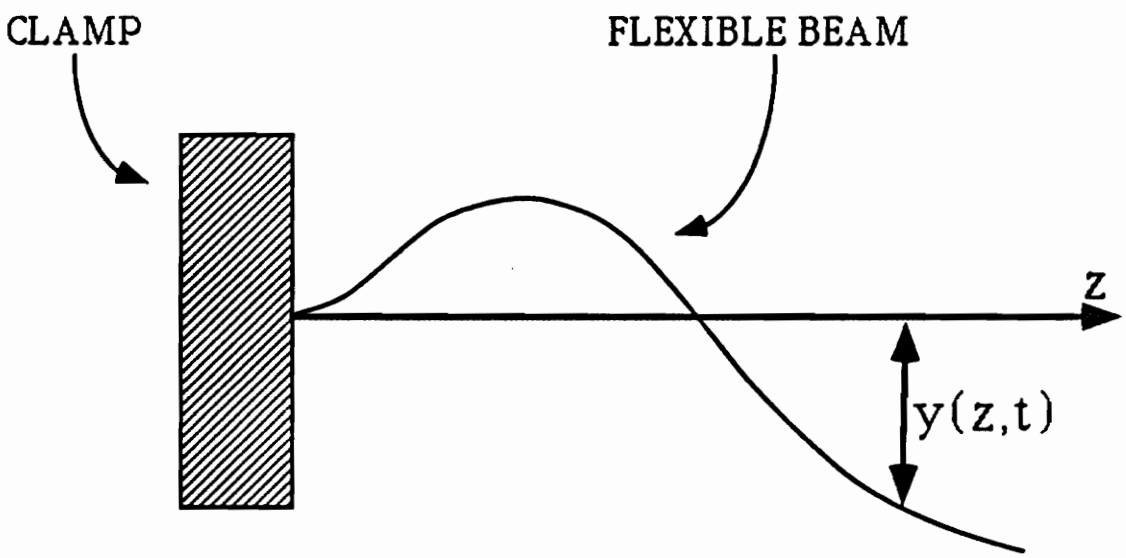

Figure 8. Coordinate system for beam dynamics

Equation (3.1.1) is a partial differential equation. A solution to this equation can be found by separation of variables. The displacement function, y(z,t), is decomposed into an infinite sum of the product of time dependent functions and spatially dependent functions,

$$y(z,t) = \sum_{n=1}^{\infty} \psi_n(z)\, \eta_n(t). \tag{3.1.3}$$

The functions $\psi_n(z)$ are called mode shapes and can be solved for in closed form. The functions $\eta_n(t)$ are called modal amplitudes and depend on the initial conditions. Setting (3.1.1) equal to zero, substituting (3.1.3), and rearranging terms yields,

$$\frac{1}{\psi_n(z)}\frac{\partial^4 \psi_n(z)}{\partial z^4} = \frac{-\rho_l}{E_b I_m}\eta_n(t)\frac{\partial^2 \eta_n(t)}{\partial t^2}. \tag{3.1.4}$$

The left hand side of (3.1.4) depends only on space, and the right hand side depends only on time. For this equation to be valid for all combinations of space and time it must be equal to a constant. Let this constant be denoted Λ_n^4. Setting the left hand side of (3.1.4) equal to Λ_n^4 we have

$$\frac{d^4 \psi_n(z)}{dz^4} + \Lambda_n^4 \psi_n(z) = 0. \tag{3.1.5}$$

Since this is a fourth order ordinary differential equation, the boundary conditions given in (3.1.2) are sufficient for determining solutions. Under these conditions the mode shapes, ψ_n, are given by [25]

$$\psi_n(z) = \frac{1}{\sqrt{l}}\Big[\cosh(\Lambda_n z) - \cos(\Lambda_n z) - \kappa_n[\sinh(\Lambda_n z) - \sin(\Lambda_n z)]\Big], \tag{3.1.6}$$

where

$$\kappa_n = \frac{\cos(\Lambda_n l) + \cosh(\Lambda_n l)}{\sin(\Lambda_n l) + \sinh(\Lambda_n l)}, \tag{3.1.7}$$

and the characteristic values, Λ_n, satisfy

$$1 + \cos(\Lambda_n l)\cosh(\Lambda_n l) = 0. \tag{3.1.8}$$

These mode shapes form a basis for the function space in which the beam's vibrations are restricted. Therefore, any beam shape can be described by a weighted sum of mode shapes. The mode shapes are orthogonal to one another, and normalized such that their inner product is unity, i.e.

$$\int_0^l \psi_i(z)\psi_j(z)dz = \delta_{ij}, \tag{3.1.9}$$

where δ_{ij} is the Kronecker delta function, defined

$$\delta_{ij} = \begin{bmatrix} 1 & \text{when i=j} \\ 0 & \text{otherwise} \end{bmatrix}. \tag{3.1.10}$$

This property of orthogonality is useful in obtaining independent differential equations for each mode. Substituting the separation of variables description for y(z,t) into (3.1.1), multiplying by $\psi_n(z)$, and integrating over the beam's length results in an ordinary differential equation which depends only on mode n. In order to define a finite dimensional model only a finite set of modal equations can be considered. This analysis considers all modes below order N. By defining a vector of modal amplitudes

$$\eta(t) = [\eta_1(t)\ \eta_2(t)\ \eta_3(t) \ldots \quad \eta_N]^T, \tag{3.1.11}$$

the resulting ordinary differential equations can be expressed in matrix form as

$$M\ddot{\eta}(t) + K\eta(t) = 0, \tag{3.1.12}$$

where

$M^{ij} = \rho_l l \delta_{ij}$,

$K^{ij} = E_b I_m l \Lambda_i^4 \delta_{ij}$, and

$\ddot{\eta}(t)$ = second derivative of $\eta(t)$.

The superscripts denote the matrix entry in row i, column j. Equation (3.1.12) describes the time dependence of the first N vibrational modes. This description assumes no natural damping. The actual system will have a small amount of damping, and experimental tests must be performed to determine the amount present. The effect of damping can be included in the model by adding a term to (3.1.12) which is proportional to $\dot{\eta}$, the modal velocities. The dynamic equation becomes,

$$M\ddot{\eta}(t) + D\dot{\eta}(t) + K\eta(t) = 0. \tag{3.1.13}$$

Since damping in the modes is uncoupled, D is a diagonal matrix. It is traditional to define a damping factor, ζ_i, which is restricted to values between zero and one. When ζ_i=0, $\eta_i(t)$ is a pure sinusoid and when ζ_i=1, $\eta_i(t)$ is a pure exponential. For values of ζ_i between zero and one, $\eta_i(t)$ is a decaying sinusoid. The matrix D can then be defined as,

$$D^{ii} = 2\,\zeta_i\,\sqrt{K^{ii}\,M^{ii}}. \tag{3.1.14}$$

Equation (3.1.13) defines a finite dimension model for the unforced vibrations of a clamped-free beam.

3.2 SENSOR MODEL

The modal domain sensor has a bandwidth far above the structural vibrations of interest. Therefore, the system model does not need to consider dynamics introduced by the sensor. Loading effects can also be neglected since the fiber is small and light compared to the structure. In Chapter 2 it was shown that the modal domain sensor produces a signal proportional to the sine of integral strain. Within a limited operating range the effect of the sine term can be linearly approximated. From (2.4.14) we have,

$$\tilde{y}_{md}(t) = I_o \Delta\tilde{\beta} \int_{f^-}^{f^+} \epsilon(z,t)\, dz. \tag{3.2.1}$$

where,

f^+, f^- = upper and lower end points of the fiber sensor,
I_o = maximum intensity of the nonlinear fiber signal, and
$\epsilon(z,t)$ = axial strain distribution along the fiber.

Under ideal bonding conditions and negligible fiber diameter, the strain in the fiber is equal to the strain at the surface of the beam. This surface strain is proportional to the beam's curvature, and is given by

$$\epsilon(z,t) = \frac{t_b}{2} \cdot \frac{\partial^2 y(z,t)}{\partial z^2}. \tag{3.2.2}$$

Using the modal decomposition for y(z,t), and substituting (3.2.2) into (3.2.1) yields,

$$\tilde{y}_{md}(t) = \frac{I_o t_b \Delta\tilde{\beta}}{2} \int_{f^-}^{f^+} \sum_{n=1}^{N} \psi_n''(z)\, \eta_n(t)\, dz = \frac{I_o t_b \Delta\tilde{\beta}}{2} \sum_{n=1}^{N} \left[\psi_n'(f^+) - \psi_n'(f^-)\right] \eta_n(t). \tag{3.2.3}$$

Since the time dependence of $\tilde{y}_{md}(t)$ is determined by $\eta_n(t)$ we can write,

$$\tilde{y}_{md}(t) = \sum_{n=1}^{N} c_n \eta_n(t), \tag{3.2.4}$$

where

$$c_n = \frac{I_o t_b \Delta\tilde{\beta}}{2}\left[\psi_n'(f^+) - \psi_n'(f^-)\right]. \tag{3.2.5}$$

3.3 ACTUATOR MODEL

Piezoelectric ceramics are crystal structures which produce a voltage when strained, or conversely produce a strain when voltage is applied. During manufacture the dipole elements within the ceramic are aligned by the application of a high voltage. This process is referred to as poling, and the axis along which this voltage is applied is called the poling axis. When small voltages are applied along the poling axis the piezoelectric will contract or expand, depending upon the voltage's polarity. Typically, piezoelectric actuators are plates which are polled along their thin axis.

In order to use a piezoelectric as an actuator the material was bonded to the surface of the beam. The geometry considered here is called a bending motor. A patch of piezoelectric material was bonded to either side of the beam, near the clamped end. By reversing the positive poling axis of each piezoelectric an applied voltage will cause one patch to expand, and the other to contract. When a voltage is applied to the surface of each patch, shear forces are transferred to the beam. Under ideal bonding conditions these distributed forces reduce to point moments at the boundaries of the piezoelectric patch. Figure 9 shows the effect of applying voltage to a piezoelectric bending motor.

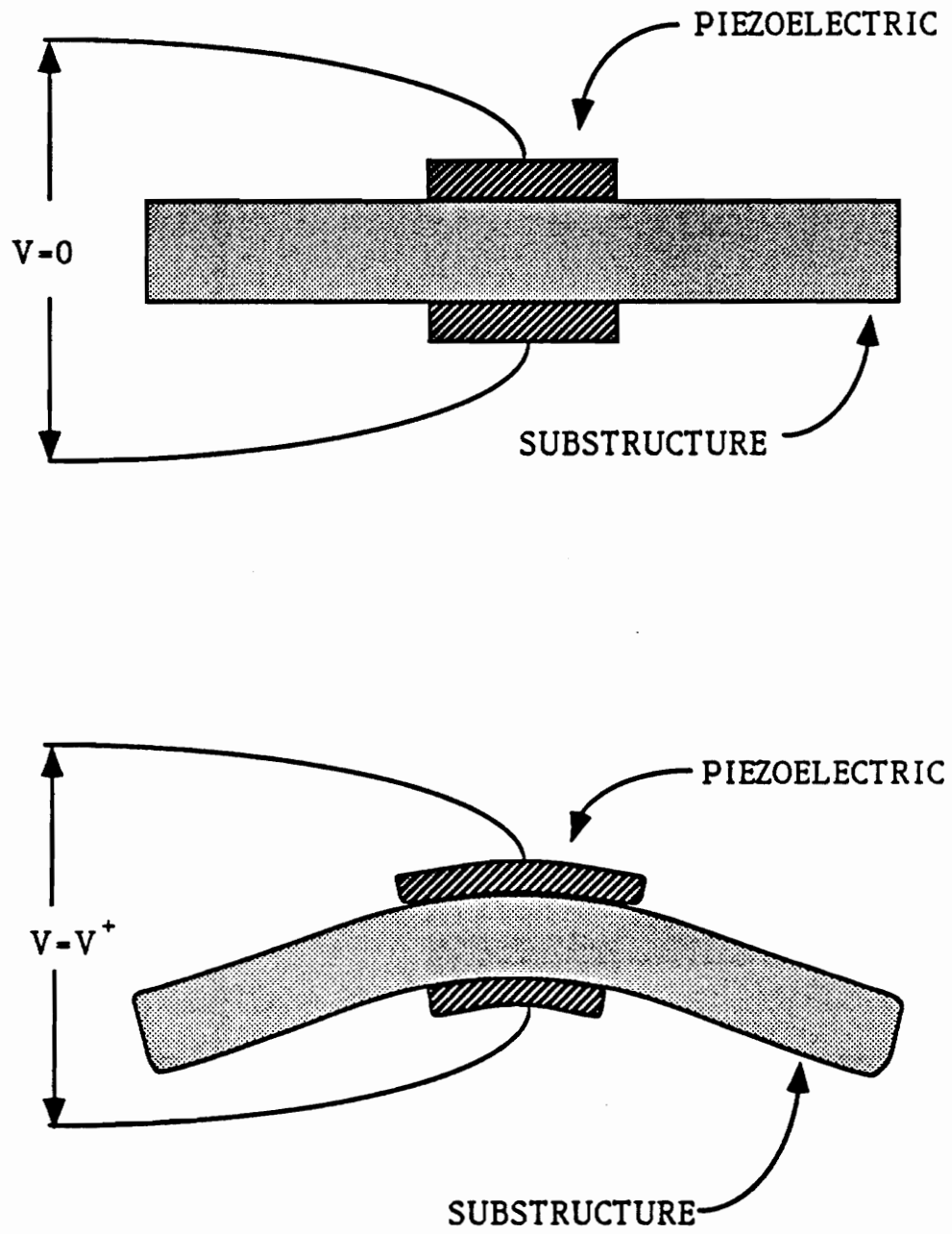

Figure 9. Operation of piezoelectric bending motor

In general, the system model must contain information about actuator dynamics. In the case of piezoelectrics, however, the frequency response is flat below the material's natural resonance. Ceramic piezoelectrics have a very high resonant frequency, compared with the frequencies of the beam's structural vibrations. Therefore, the actuator's dynamic response can be ignored in the system model. Furthermore, since the patch is light compared with the mass of the beam, loading effects can be neglected. The system model need only consider the added stiffness, and the effect of applied forces from the piezoelectric patch. The added stiffness is modelled by adjusting the stiffness matrix, K, derived in Section 3.1. Forces applied from the piezoelectric are modelled as an input to (3.1.13).

Bonding piezoelectric patches to the beam changes the beam's stiffness in the area of the patch. This additional passive stiffness can be modeled by considering the addition of strain boundary conditions at the edge of the piezoelectric patch. For a perfectly bounded actuator the additional stiffness is given by [26],

$$K_p^{ij} = \frac{E_b t_b^3 h_b}{2l^2\left[6+\frac{E_b t_b h_b}{E_p t_p h_p}\right]}\left[\psi_i''(p^+)\psi_i'(p^+) - \psi_i''(p^-)\psi_i'(p^-)\right], \qquad (3.3.1)$$

where

p^+, p^- = upper and lower end points of the piezoelectric,
E_b, E_p = Young's modulus for the beam and piezoelectric,
t_b, t_p = thickness of the beam and piezoelectric,
h_b, h_p = height of the beam and piezoelectric, and
ψ', ψ'' = first and second derivatives of $\psi(z)$.

The influence that the piezoelectric patch has on each mode of the beam is

determined by the modal force vector, Q. The dynamics of a forced beam are described by setting (3.1.13) equal to Q(t). When the external forces are moments the elements of the modal force vector are given by,

$$Q_i(t)=\int_0^l M_o(z,t)\psi_i''(z)\,dz, \tag{3.3.2}$$

where $M_o(z,t)$ is a moment distribution.

The piezoelectric patch applies a uniform shear force along its length. When two patches are used in a bending configuration the resulting moment is given by the shear force created times the beam's thickness. The force generated by a bonded piezoelectric depends upon the substructure material, as well as the piezoelectric material. A full analysis is presented in [27]. The moment distribution considered here is given by,

$$M_o(z,t) = \frac{E_b\, t_b^2\, h_p}{\frac{E_b t_b h_b}{E_p t_p h_p} + 6} \cdot \frac{d_{31}}{t_p}\, v(t)\,, \quad \text{for } p^- < z < p^+ \tag{3.3.3}$$

where,

d_{31} = piezoelectric charge constant, and

$v(t)$ = voltage applied to each piezoelectric.

This moment yields a modal force,

$$Q_i(t) = \frac{E_b\, t_b^2\, h_p}{\frac{E_b t_b h_b}{E_p t_p h_p} + 6} \cdot \frac{d_{31}}{t_p}\left[\psi_i'(p^+) - \psi_i'(p^-)\right] v(t) = q_i v(t). \tag{3.3.4}$$

The time dependance of the modal force is given by the applied voltage, v(t). The matrix equations for the beam-actuator system can now been written,

$$M\ddot{\eta}(t) + D\dot{\eta}(t) + (K+K_p)\eta(t) = Qv(t), \tag{3.3.5}$$

where $Q \equiv [q_1\ q_2 \ldots q_N]^T$.

Equation (3.2.4), and (3.3.3) form a complete model for the instrumented beam. This model, consists of a set of independent second order differential equations. By defining a state vector, $x=\begin{bmatrix}\eta\\ \dot{\eta}\end{bmatrix}$, the N second order equations can be written as 2N first order differential equations. The state equations are,

$$\dot{x} = \begin{bmatrix} 0 & I \\ -M^{-1}(K+K_p) & -M^{-1}D \end{bmatrix} x + \begin{bmatrix} 0 \\ M^{-1}Q \end{bmatrix} v(t) \equiv Ax + Bv. \tag{3.3.6}$$

$$\tilde{y}_{md}(t) = [c_1\ c_2 \ldots\ c_N\ 0\ 0 \ldots\ 0]x \equiv Cx, \tag{3.3.7}$$

These equations form the complete linear model for the instrumented flexible beam.

4.0 SYSTEM DESIGN

This chapter describes the construction of the flexible beam experiment, and the development of a dynamic compensator. The first section discusses some of the sizing constraints and gives the dimensions of the beam, actuator, and sensor. Section 4.2 details the optical hardware which was utilized in constructing the modal domain sensor. The analog circuitry associated with the sensor is described in Section 4.3. Section 4.4 is concerned with the use of piezoelectric ceramics as actuators. The placement and bonding of the piezoelectric bending motor is discussed. Section 4.5 describes the construction of a compensator for the experiment. Phase compensation is used to design a fourth order, output feedback control law. The differences between the actual system and linear system model are addressed in Section 4.6. The linear continuous model is shown to be suitable for design purposes.

4.1 PHYSICAL PARAMETERS

Many sizing considerations must be made in the design of the experiment described in Chapter 1. The beam's parameters must be chosen such that none of

the modeling assumptions are violated. The beam must exhibit vibrations in only one dimension. These vibrations must also remain small, in order for the sinusoidal nonlinearity in the sensor's signal to be neglected. The beam's vibrations should be low frequency, and have very little natural damping. These properties are typical of the dynamics of large flexible structures. Low frequency vibrations also allow for sampling rates which can be achieved with a general purpose digital computer. The actual size and stiffness of the beam must be designed such that commercially available piezoelectrics can influence the vibrations.

Trade-offs between the sizing considerations are complex, and impossible to evaluate quantitatively. A suitable design was arrived at through iteration. The final system parameters are listed in Table 1. A program was written to generate the state space system model from a set of parameters. The program listing is given in Appendix A. This model was then tested by simulating step responses, and the response to excitation at modal frequencies. The tip displacement, fiber signal, and piezoelectric voltage were studied for each of these tests. Once a design was found which meet the sizing requirements, the experiment was constructed.

4.2 SENSOR HARDWARE

In order to eliminate the second mode's spatial degeneracy, elliptical core fiber was used for the dual mode fiber sensor. The fiber chosen for this experiment has the specifications listed in Table 2. These fibers exhibit a stable two lobe pattern when operated at a wavelength of 633 nm. Qualitatively, the

TABLE 1. SYSTEM PARAMETERS

Beam material	Steel
Young's modulus, E_b	200 GPa
Density, ρ	7860 Kg/m^3
Length, l	0.614 m
Height, h_b	0.05 m
Thickness, t_b	0.74 mm
Piezo height, h_p	0.0317 m
Fiber end points:	
f^-	0.0 m
f^+	0.566 m
Piezo end points:	
p^-	0.012 m
p^+	0.05 m

TABLE 2. FIBER SPECIFICATIONS

Manufacture	Andrew Corporation
Product type	E- Series, 48280-1-P
Operating wavelength, λ	850 nm
Core size	1μm x 2μm ellipse
Cladding size	40 μm radius
Coating size	60 μm radius
Core index, n_1	1.458
Cladding index, n_2	1.453
Fiber adhesive	M-Bond 200 Measurements Group, Inc

dual mode elliptical core fiber behaves like a circular core fiber with only the LP_{01} and LP_{11} even modes propagating, as described in Chapter 2.

The modal domain sensor is used to detect strain along the beam's length. Additional fiber was required to guide the light from the laser to the beam, and from the beam to the photodetector. Small disturbances to these sections of fiber would cause variations in the sensor's signal that were not related to the beam's vibrations. To eliminate this problem nonsensing fibers were fused to either end of a sensing fiber. The fusion splicing created a modal domain sensor which was only sensitive to strain in a central region [28]. Figure 10 shows the complete, three section modal domain sensor. The sensing section of this fiber was bonded to the beam from the clamp to the beam's free end, using a high stiffness epoxy.

The nonsensing leads were single mode optical fibers. When a fiber supports only one mode, no interference effects occur. Therefore, the output intensity of a single mode fiber remains constant under applied strain. To maintain steady launch conditions in the dual mode fiber, the polarization of light must remain stable in the single mode lead-in fiber. Typically strain will cause the polarization in single mode fibers to shift. To keep the polarization shift from affecting the sensor's output, a polarization preserving fiber must be used as the lead-in section. Single mode elliptical core fiber was used. It is polarization preserving, and creates an efficient splice when fused to the elliptical core dual mode fiber.

Single mode 633 nm circular core fiber was used for the insensitive lead-out section. To obtain an amplitude modulated signal, from the phase modulated signal in the dual mode fiber, required a spatial filter. The filter must block light

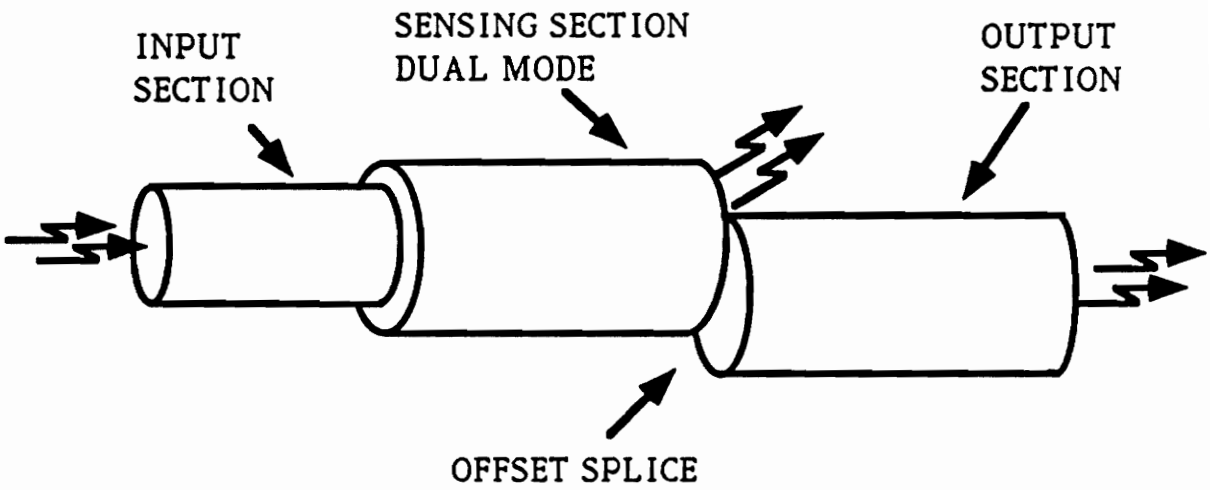

Figure 10. Optically spliced modal domain sensor

from half the core, while passing the rest of the intensity pattern to a photodetector. This filtering operation was accomplished in line with an offset fusion splice. The circular core fiber was misaligned with the elliptical core dual mode fiber, when the fibers were fused together. The fusion was performed while the dual mode fiber was actively sensing strain. The degree of misalignment was adjusted until an optimal modulation depth was found. This fiber formed a insensitive lead-out section, and completed the construction of the modal domain sensor.

The signal from the modal domain sensor is a nonlinear function of strain. It is desirable to operate the sensor around the quadrature point where the signal is most nearly linear. To place the fiber at quadrature, at zero structural strain, requires the application of a static prestrain. In the experiment the beam and sensor were extended through the back of the clamp. A static stain was applied to the fiber by displacing the tip of the beam's extended section. This arrangement is shown in Figure 11.

4.3 SIGNAL PROCESSING

The sensor's signal required some electronic processing before it could be sampled by the digital controller. A photodetector circuit was used to convert the optical signal into an analog voltage. This voltage contained a DC bias when the fiber was set at quadrature. To remove the bias a high pass analog filter was constructed which had a cutoff frequency well below the first mode of the beam. Shot noise and thermal noise in the photodetector circuit added wideband noise to

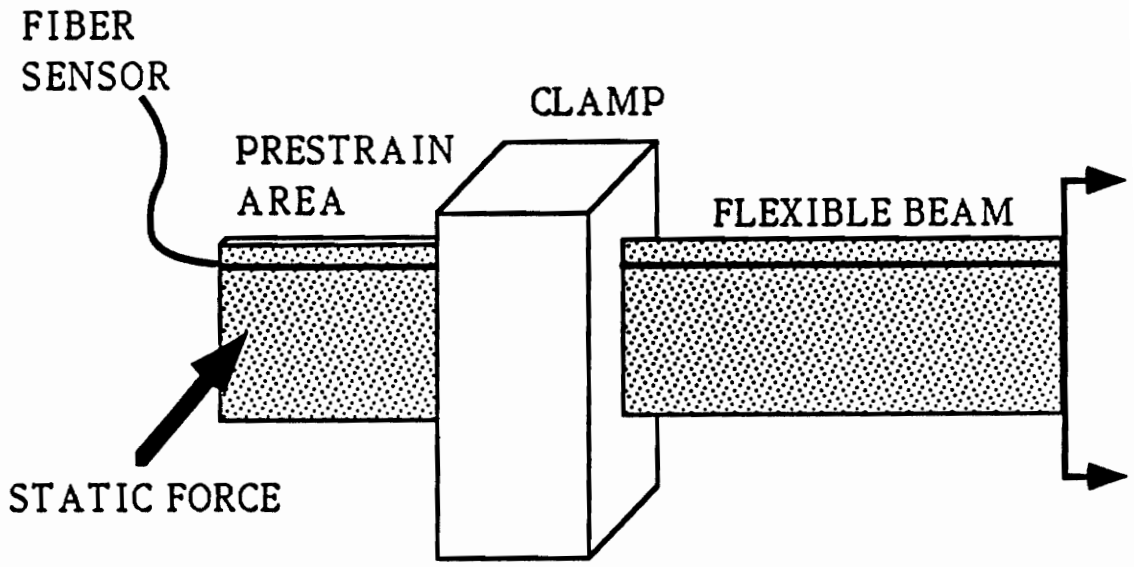

Figure 11. Prestrain device to set quadrature point

the fiber's signal. To avoid aliasing problems with the digital compensator, a low pass filter was also required. Both filters were implemented as a bandpass circuit, utilizing a single operational amplifier. The circuit diagram is given in Figure 12. From an input-output perspective, the dynamics of the signal conditioning circuitry appear as dynamics of the system. In order to accurately simulate the response of the system the dynamics introduced by the filtering circuitry must be considered. The state space equations which describe the filter operation are,

$$\dot{x} = \begin{bmatrix} -1000 & -454.5 \\ 1 & 0 \end{bmatrix} x + \begin{bmatrix} 1 \\ 0 \end{bmatrix} \tilde{y}_{md}, \tag{4.3.1}$$

$$\tilde{\tilde{y}}_{md}(t) = \begin{bmatrix} 1000 & 0 \end{bmatrix} x,$$

where $\tilde{\tilde{y}}_{md}$ is the filtered fiber signal. These equations were appended to the original modeling equations, and included in the simulation.

The digital controller only provided control signals at discrete points in time. In between samples the analog to digital converter held the control voltage constant. Due to the high bandwidth of the piezoelectric actuator, discontinuities in the control signal excited high order modes in the beam. A low pass filter was used to smooth the output from the A/D converter and amplify the signal. The cutoff frequency of the smoothing filter was approximately seven times the Nyquist frequency of the digital controller. Its effect on the system dynamics was negligible, so it was not considered in the simulation.

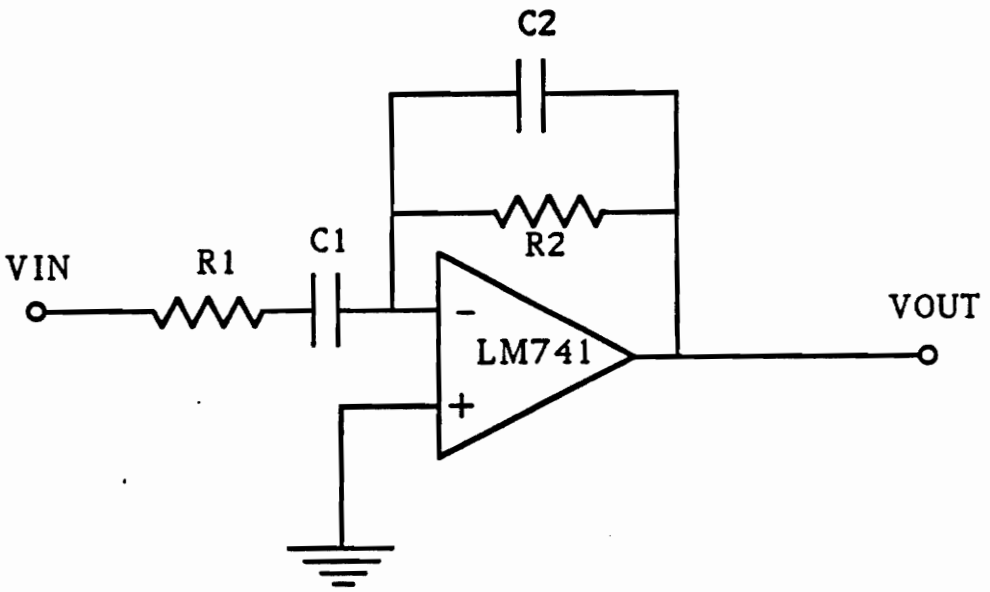

R1 = 10 K
C1 = 220 μF
R2 = 100 K
C2 = 0.01 μF

Figure 12. Circuit diagram for signal conditioning electronics

4.4 ACTUATOR HARDWARE

A piezoelectric bending motor was used to excite and control the beam's low frequency modes. The specifications for this material are listed in Table 3. A patch of piezoelectric ceramic was bonded to either side of the beam. A thin copper film was soldered to the backside of each piezoelectric. These contacts were connected to ground. The outer surfaces of the piezoelectrics were electrically connected, and wired to the driving signal.

Piezoelectric actuators rely on the transfer of strain from the piezoelectric patch to the beam. The effect of strain transfer on the beam is determined by the integral of the strain in the beam's mode shapes. In areas where a mode shape has a high average strain, the piezoelectric patch will be effective in exciting that mode. If the piezoelectric patch is located evenly about a strain node for a particular mode, it will not be able to excite that mode. In this experiment only the low order modes of a cantilevered beam were to be controlled. Since only one actuator was being used it was placed as close to the root as possible. This placement was optimum for the first mode, and avoided strain nodes of the low order modes.

Thick or pliable bonding layers introduce a lag in the transfer of strain from the piezoelectrics. To approximate a perfect bond the piezoelectrics were bonded with a thin stiff epoxy. The epoxy was mixed, and then placed in a vacuum chamber for approximately five minutes. The low pressure caused the epoxy to boil off air bubbles which were introduced in the mixing. The epoxy was then spread in an even layer on the piezoelectric. Weights were used to maintain a constant pressure on the piezoelectric while the epoxy cured.

TABLE 3. PIEZOELECTRIC SPECIFICATIONS

Manufacturer Product type	Piezo Systems G-1195
Material Charge constant, d_{31} Young's modulus, E_p Thickness, t_p Height, h_p	Lead Zirconate Titanate 0.166 μm/Kilovolt 630 GPa 190 μm 0.0381 m
Piezoelectric Adhesive	BA-F253 Tra-Con Inc.

4.5 COMPENSATOR DESIGN

With the parameters listed in Table 1, and the modeling equations described in Chapter 3, a numerical state space system model was developed. A control law can be designed, based on this model, which utilizes compensated sensor feedback to suppress vibrations in the beam. The goal of this research, was to demonstrate the use of a fiber sensor in a closed loop control system, and accurately verify the modeling procedure. Since optimizing the system's closed loop performance was not of interest a simple design procedure was chosen.

The beam has only one actuator, the piezoelectric patch, and one sensor, the optical fiber. Such single input, single output systems can be represented by a transfer function in the Laplace domain. The conversion from a state space representation to a transfer function is given by

$$G(s)=C(sI-A)^{-1}B, \tag{4.5.1}$$

where I is the identity matrix. The control system was to add damping to the structure. For this experiment only the first four modes were considered significant. Therefore, the design model only contained four modes. The effect of the analog filters, and sensor nonlinearity were not included in the design model. These effects are addressed in Section 4.5. The transfer function for the design model is

$$G(s)=\frac{9.28\text{x}10^{-5}(s+14.9)(s-14.9)((s+128)^2+99^2)((s-128)^2+99^2)}{((s+.03)^2+10.5^2)((s+.11)^2+65.2^2)((s+.29)^2+181^2)((s+.46)^2+354^2)}. \tag{4.5.2}$$

The poles of this system have very small negative real parts, which

corresponds to a system with little damping. Under simple gain feedback the poles have a departure angle, in the imaginary plane, of $\pm 90^{\circ}$. This departure angle means gain feedback causes a shift in the frequency of the poles, but add no damping to the system. To achieve maximum damping at low gains, the poles should have a departure angle of 180°. The response at low gains is important because the piezoelectric actuators have relatively low authority. A procedure called phase compensation was used to design the control law [29]. The departure angle is adjusted by the phase of the compensator, at the frequency of the pole. Therefore, the ideal compensator would have a phase characteristic which shifted from -90° at the frequency of one system pole to 90° at frequency of the next system pole. This type of phase response can be obtained by a pair of complex zeros, and a pair of real poles at the same frequency. The transfer function is,

$$H(s)=\frac{(s^2+ w_o^2)}{(s + w_o)^2}. \tag{4.5.3}$$

A filter of this type has a phase response which shifts abruptly from -90° to 90° at the frequency w_o. A compensator for the four mode system could simply be two filters, with the frequencies, w_o, falling in between the first and second modes, and the third and fourth modes. The first filter would affect the departure angle of the first and second mode, while the second filter would compensate the third and fourth mode.

This design procedure addresses the phase requirements of the compensator, but does not specify the magnitude characteristics. Since the settling time of the system is dominated by the first mode's response, it is desirable to have higher damping in the first mode. Making the magnitude response of the compensator

higher at low frequencies gives it more authority over the first mode. It is also desirable that the compensator does not affect modes which are not included in the system model. Since the high frequency modes were neglected, the compensator should have a magnitude response which decreases at higher frequencies.

These magnitude characteristics can be obtained by placing the poles of each filter closer to the origin. Doing this, however, tends to spread the filter's phase transition over a larger frequency range. In the first filter the phase variation was not a problem. However, phase contributions from the second filter were found to adversely affect the departure angle of the second mode. To sharpen the phase transitions of the second filter its double real pole was moved into the complex plane. It was placed closer to the origin, with equal real and imaginary parts. The final compensator design was

$$H(s)=\frac{(s^2+40^2)(s^2+300^2)}{(s+35)(s+40)((s+150)^2+150^2)}. \qquad (4.5.4)$$

The frequency response of the compensator is shown in Figure 13.

A root locus shows the pole locations of a closed loop system for increasing values of gain. Figure 14, shows the root locus for the compensated beam. The pole locations for a reasonable gain choice are marked by boxes on the loci. Under compensated feedback all the closed loop poles have more damping than in the open loop system.

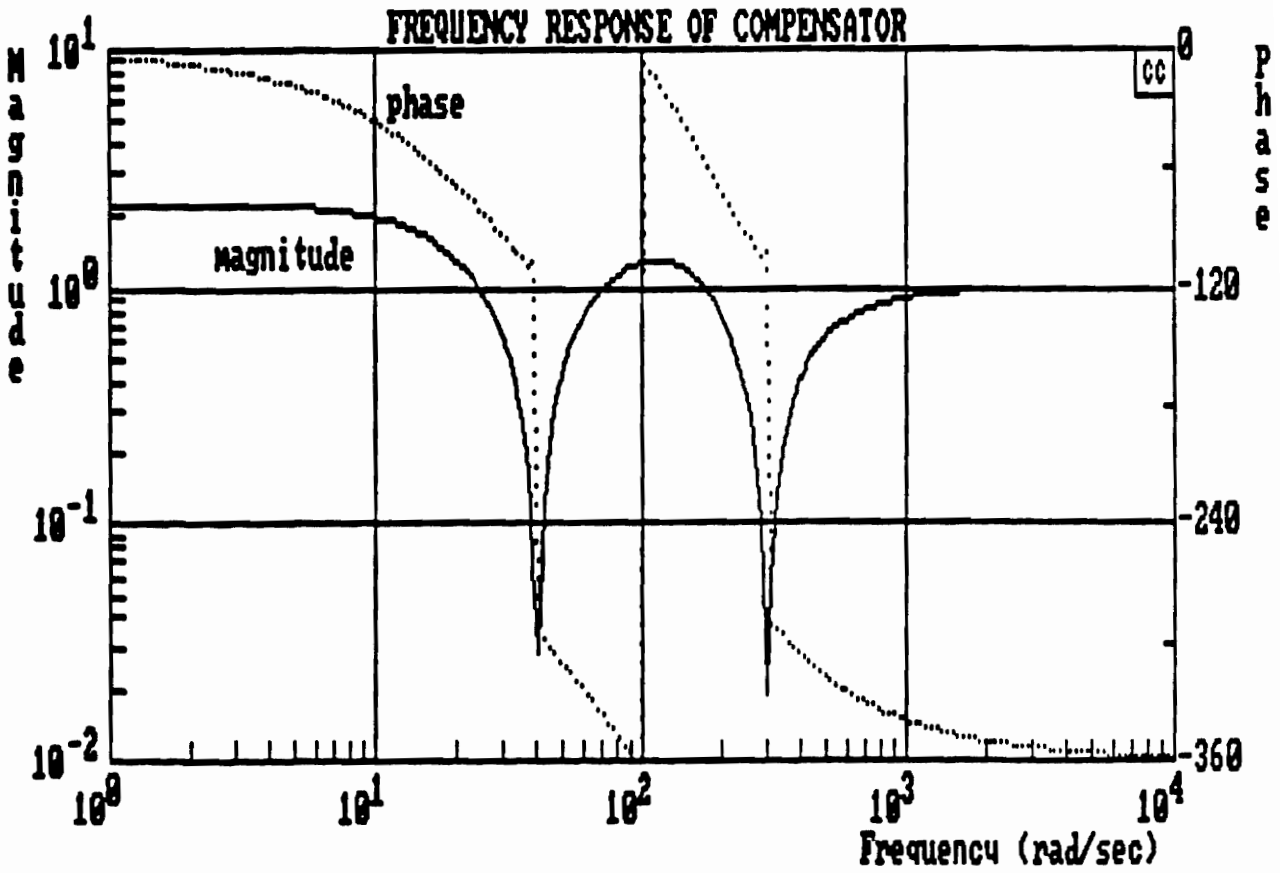

Figure 13. Frequency response of compensator

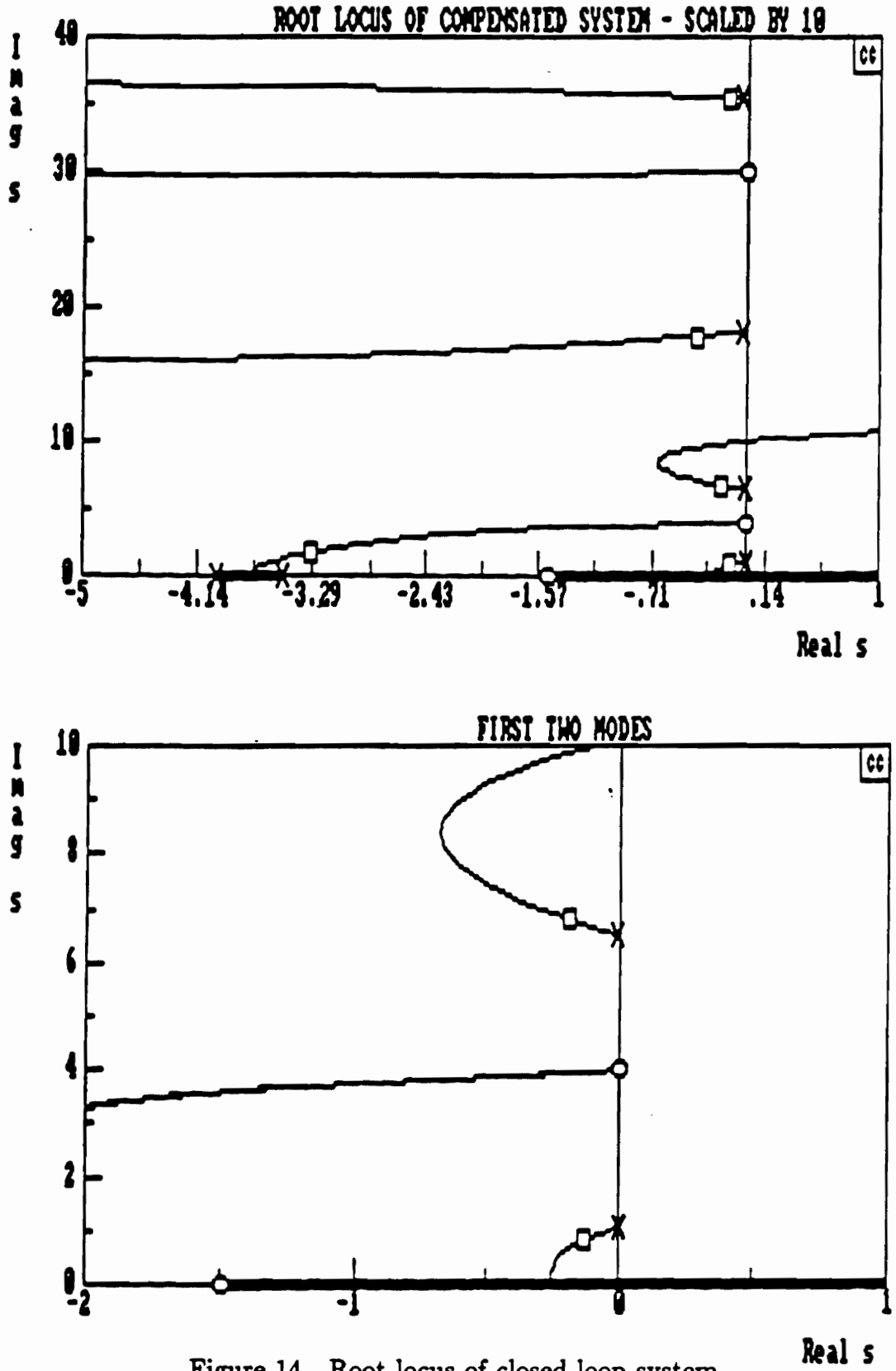

Figure 14. Root locus of closed loop system

4.6 PERFORMANCE EVALUATION

Four major approximations were made in the design of the control law. First, the modal domain sensor was assumed to have a linear dependance on strain. The signals dependance is actually sinusoidal, and this approximation is only valid at small strain levels. Second, the saturation of the actuator was ignored. At large voltages the piezoelectric will begin to depole, and consequently lose its effectiveness. To maintain a consistent response from the piezoelectric actuator, the control signal was amplitude limited. Third, the compensator was designed in the continuous domain, although in practice a digital computer was used to implement the control law. The compensator was mapped into the digital domain using a zero order hold equivalence, at a sampling time of 2.19 milliseconds. Aliasing, and the effect of executing the compensator as a difference equation were ignored. Finally, the dynamics of the detection electronics were not included in the design model.

The reduction in complexity resulting from these assumptions greatly simplified the compensator design. In evaluating the performance of the compensator, however, all these effects must be considered. A simulation program was used to test the closed loop system, and predict the effectiveness of a control law. The model used in simulation is called the truth model since it considered the effect of nonlinearities, sampling, and analog filtering. Code and documentation for the simulation are given in Appendix B. In order to justify the use of a simplified design model the closed loop response of the design model was compared to that of the truth model. The initial conditions specified amplitudes in all four modes of the beam, and these amplitudes were large enough to produce a nonlinear signal from the sensor. Furthermore, a high gain was chosen so the

actuator would experience saturation. Figure 15 shows the simulated closed loop response of the design model and truth model. There is a slight difference in closed loop frequencies. This variation is probably due to the sensor's nonlinearity, and its effect on the closed loop gain. However, the differences are small enough to justify the use of a simplified model for the compensator design.

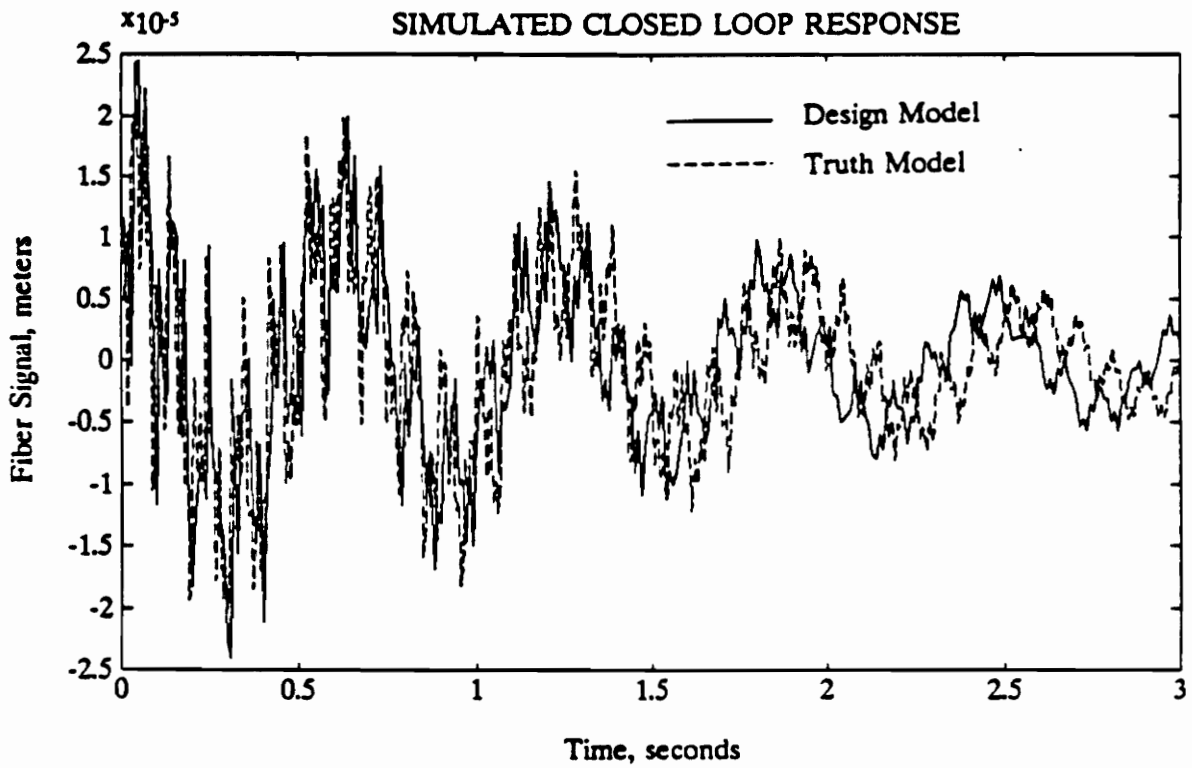

Figure 15. Closed loop response of design model and truth model

5.0 RESULTS

In this chapter the experimental and simulated results of a series of dynamic tests on the flexible beam are presented. The first four sections are concerned with open loop verification of the system model. Section 5.1 discusses the use of a system identification routine to verify the frequencies of the beam's first four modes. The damping present in each of these modes is also determined, and included in the system model. Section 5.2 describes the calibration procedure used to verify the fiber's sensitivity. The authority and linearity of the actuator are tested in Section 5.3. The open loop system response is compared to simulations for a variety of inputs in Section 5.4. The last section presents closed loop response of the system to various inputs. These results are compared to the open loop system, as well as to the simulated response.

5.1 FREQUENCY RESPONSE

To verify the beam's dynamic model, the frequency response of the actual system was compared to that of the model. A system identification technique, known as the empirical transfer function estimate, was utilized to generate the

experimental frequency response [30]. An estimate of the system's frequency response was obtained from a spectral ratio of input and output signals. The accuracy of this estimate depends upon the uniformity of the input signal's frequency spectrum and the amount of noise in the output signal.

Electric signals were applied to the piezoelectric to excite vibrations in the beam. Impulse, square wave, and random noise input signals were used to assure wideband excitation. The input and output signals were stored by a digital computer. Discrete Fourier transforms of the input and output data provided the frequency spectrum of these signals. To reduce the effect of noise this experiment was performed several times, and the results were averaged. To further account for the frequency spectrum of the input signal the average was weighted by the power in the input signal. The frequency response estimate is given by

$$G(w)=\frac{\sum_{i=1}^{n}\frac{Y_i(w)}{U_i(w)}|U_i(w)|^2}{\sum_{i=1}^{n}|U_i(w)|^2}, \tag{5.1.1}$$

where

$Y_i(w)$ = input signal's frequency spectrum,

$U_i(w)$ = output signal's frequency spectrum, and

n = number of data sets.

Figure 16 shows a comparison of the predicted frequency response to the experimentally determined frequency response. The frequencies match well for the first four modes. The frequency response estimate has a spike just above the fourth mode, which does not appear in the modelled response. This spike was due to 60 Hertz line noise in the detection electronics. The amplitude of estimated frequency spikes are not as sharp than those predicted by theory. However, the

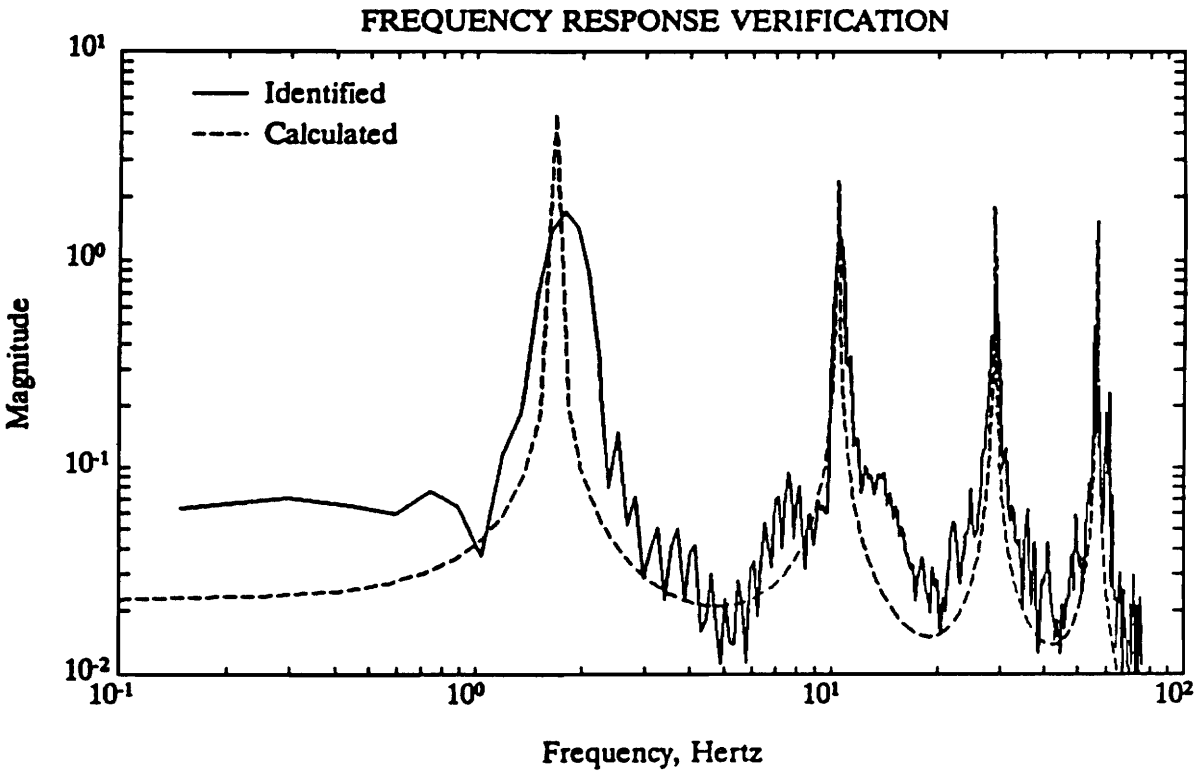

Figure 16. Experimental and predicted frequency response

system model assumed zero damping, making the response infinite at modal frequencies. To make the model more realistic a small amount of natural damping must be added.

The frequency response test provided an estimate of the modal frequencies, however, to accurately determine the damping in these modes required time domain data. The piezoelectric actuator was used to drive the beam into single frequency oscillations. Once excited the natural decay of the vibrations was recorded. The damping factor, ζ, can be found from this data using log decrement [25].

$$\zeta_i = \frac{1}{2\pi n} \log\left[\frac{a_1}{a_n}\right], \tag{5.1.2}$$

where,

a_1= amplitude of first cycle, and

a_n = amplitude of n_{th} cycle.

The natural decay of the first two modes is shown in Figure 17. Similar data was taken for the third and fourth modes. From this data damping factors were calculated, using (5.1.2). The model was then reconstructed with the damping factors listed below.

ζ_1= 0.0026

ζ_2= 0.0017

ζ_3= 0.0016

ζ_4= 0.0013

5.2 SENSOR CALIBRATION

Due to the lack of an analytical description for the elliptical core dual mode

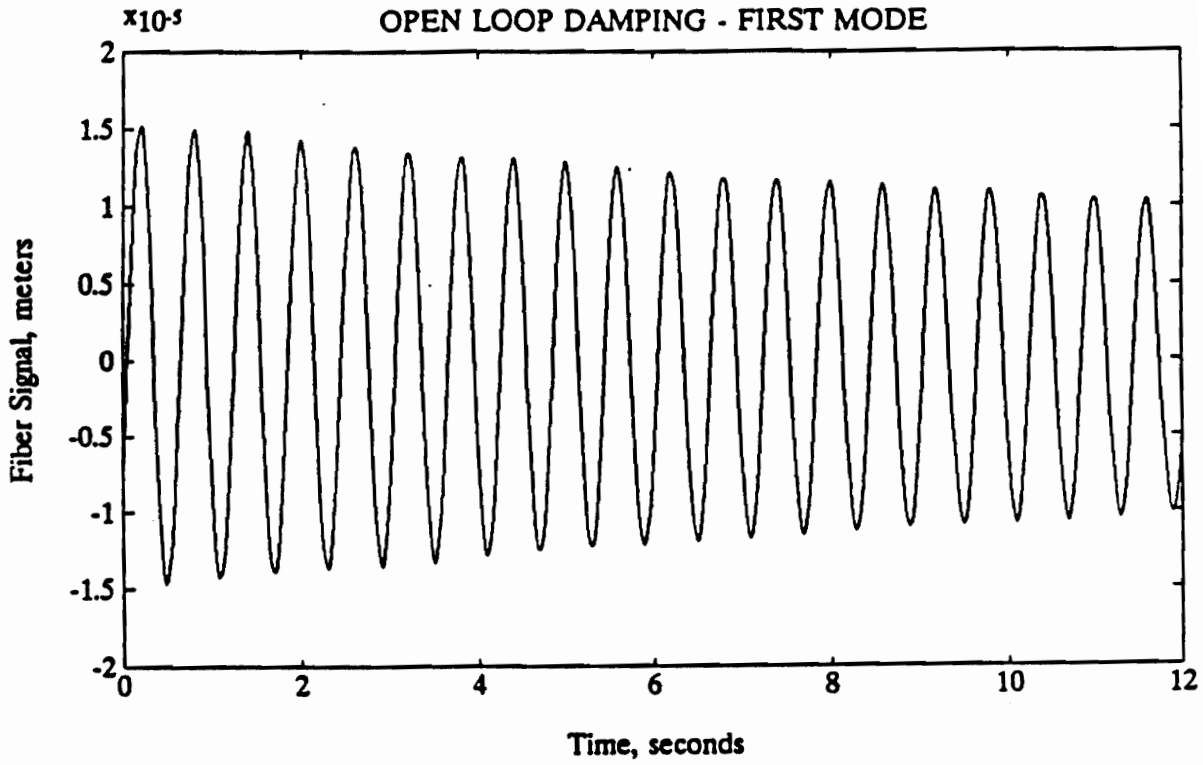

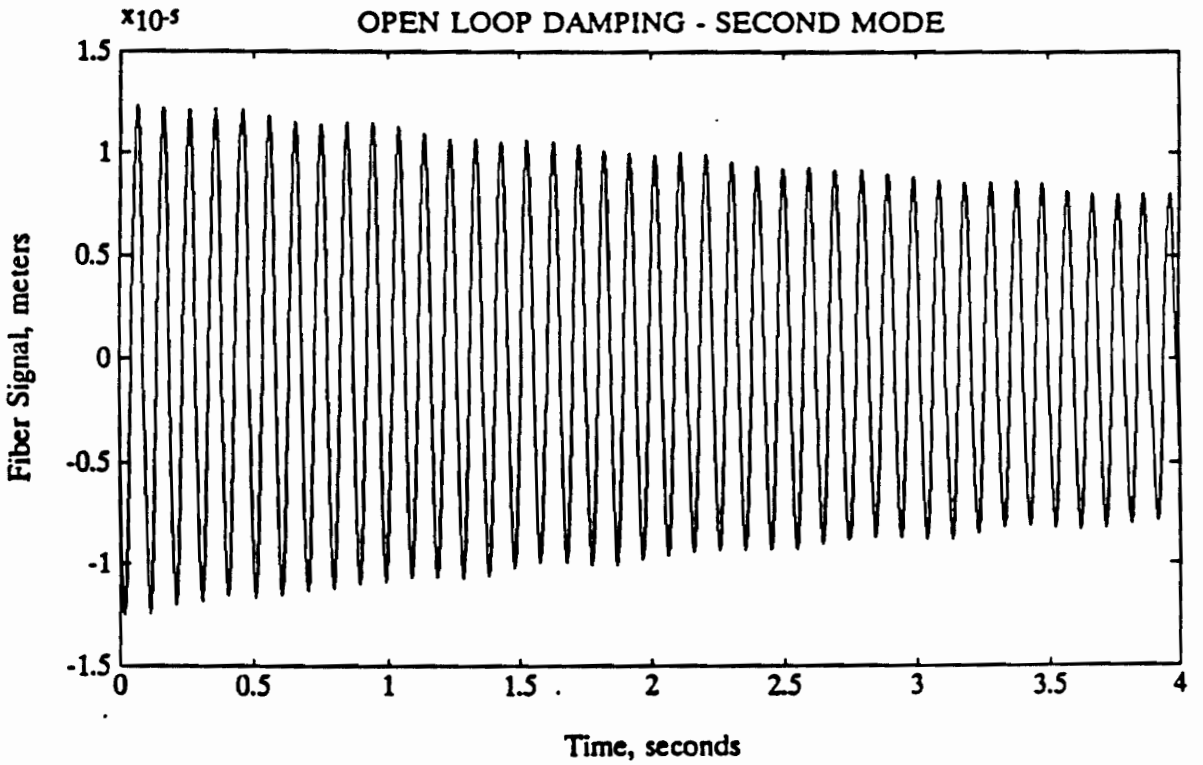

Figure 17. Natural decay of first two modes

fiber, empirical values must be used for the fiber's sensitivity. The parameter which defines the fiber's sensitivity is the fringe length, $\frac{2\pi}{\Delta\tilde{\beta}}$. Independent tests have found fringe length of 102 μm for the Andrew elliptical core fiber [28]. However, since the bonding of the fiber to the beam may not be ideal, a calibration test was performed.

The calibration test compared the predicted and experimental fiber signals from a known strain distribution. The stain distribution was generated by displacing the tip of the beam from its equilibrium position. The beam's tip was attached to a positioner, which was used to measure the tip deflection. The experimental setup is shown in Figure 18. The tip was displaced from zero to 4 centimeters, in one millimeter increments. At each step a data acquisition system recorded the fiber signal for two seconds, and averaged the data to reduce the effects of noise.

To perform this test an expression for the fiber signal as a function of tip deflection must be calculated. The displacement of a cantilevered beam due to tip loading is [31],

$$y(z)=\frac{Pz^2}{6E_bI_m}(3l-z), \tag{5.2.1}$$

where P is the force applied at the beam's tip. From (2.4.13), we have the modal domain sensor's response to strain is,

$$y_{md} = I_o \sin\left[\Delta\tilde{\beta}\,\frac{t_b}{2}\int_{f^-}^{f^+}\frac{\partial^2 y}{\partial z^2}\,dz\right]. \tag{5.2.2}$$

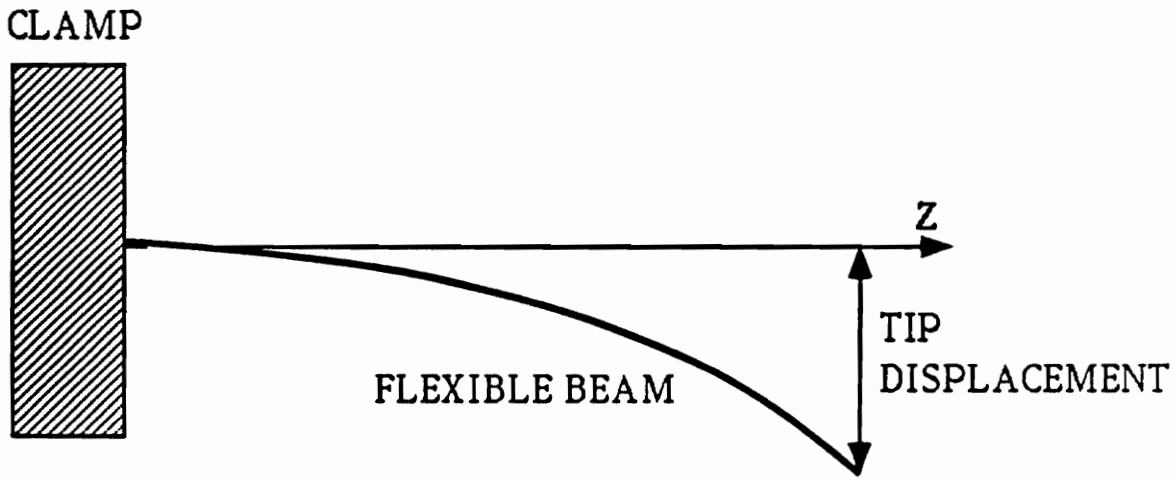

Figure 18. Tip deflection experiment

Differentiating (5.2.1) and substituting into (5.2.2) yields

$$y_{md}=I_o\sin\left[\Delta\tilde{\beta}\,\frac{t_b P}{2E_b I_m}\int_{f^-}^{f^+}(l-z)dz\right]. \tag{5.2.3}$$

Again using (5.2.1) the force, P, can written in terms of the induced tip deflection. Substituting this description for P into (5.2.3) yields,

$$y_{md}=I_o\sin\left[\Delta\tilde{\beta}y(l)\frac{3t_b}{2l^3}\int_{f^-}^{f^+}(l-z)\,dz\right]. \tag{5.2.4}$$

The graph shown in Figure 19 is a comparison of (5.2.4) with the experimental data. The data matches well up to about 22 μm of integrated strain. After this point the experimental data fails to match with the model. At this strain level the sensor's nonlinearity is significant. Since the experiment was designed to operate in the linear range, these discrepancies were not considered. During the dynamic tests the vibrations were keep well below the level corresponding to 22 μm of integrated strain.

5.3 ACTUATOR CALIBRATION

To verify the modeling of the piezoelectric actuator the magnitude of actual and simulated responses to various inputs were compared. The influence the actuator had over each mode was determined by driving the system at resonance, and comparing the response to simulation. To test the actuator for linearity, each mode was excited at three different voltage levels. When the experimental results

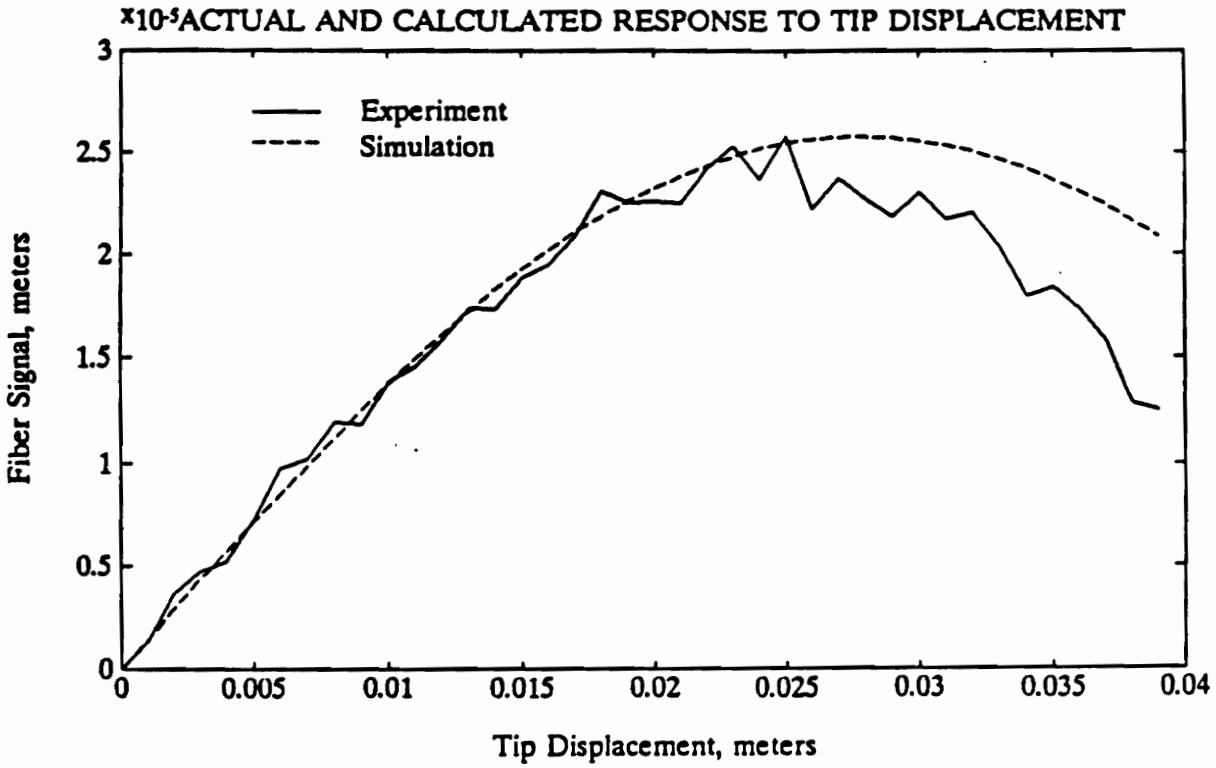

Figure 19. Experimental and predicted response to tip deflection

were compared to simulation, the signals were found to differ by a scaling factor. This scaling factor was calculated for each voltage, and each of the first three modes. These results are listed in Table 4. Since the scaling factor is the nearly same for each mode, the modeling procedure is essentially correct. The actuator also appears to be linear over the voltage range of interest. However, the piezoelectric was found to have on average 1.51 times more authority than predicted by theory.

In order to calibrate the actuator's authority, a scaling factor of 1.51 was applied to the piezoelectric charge constant. The charge constant, denoted d_{31}, relates the change in length of a piezoelectric due to an applied electric field. This factor is linearly related to the actuator's authority. Although given as a constant this parameter actually depends upon the strain and temperature history of the piezoelectric material. The charge constant provided by the manufacture was assumed to be conservative.

5.4 OPEN LOOP RESPONSE

Sections 5.1-5.3 detailed the independent testing of the beam model, fiber sensitivity, and piezoelectric authority. With these complete the final step in verifying the system model was to compare simulated and experimental input-output data. Figures 20 thru 23, compare the simulated and experimental open loop response of the system to excitation in each of the first four modes. The frequencies match fairly well, as predicted by the frequency response estimates. The damping and amplitude of excitation also match well. In the higher modes the transition from excitation to open loop causes a phase shift in the experiment,

TABLE 4. ACTUATOR SCALING FACTORS

	10 Volts	20 Volts	30 Volts
Mode 1	1.44	1.51	1.52
Mode 2	1.54	1.52	1.47
Mode 3	1.51	1.54	1.56

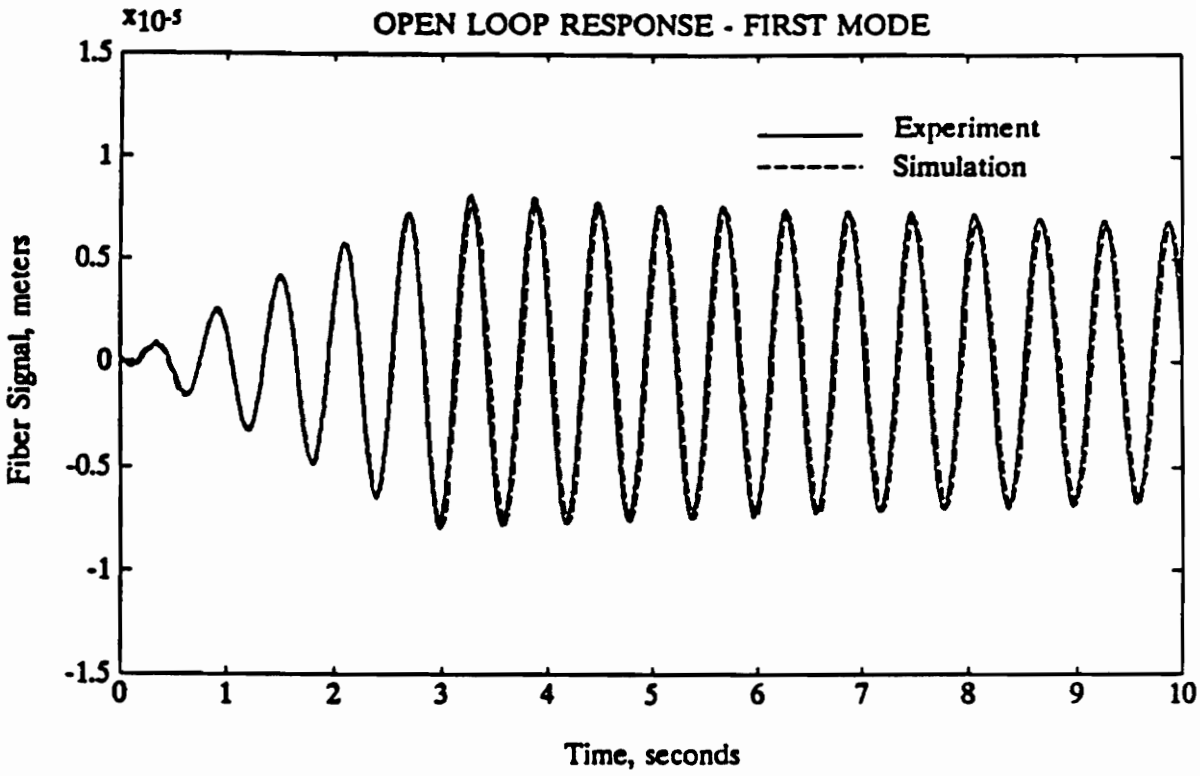

Figure 20. Simulated and experimental open loop response, first mode

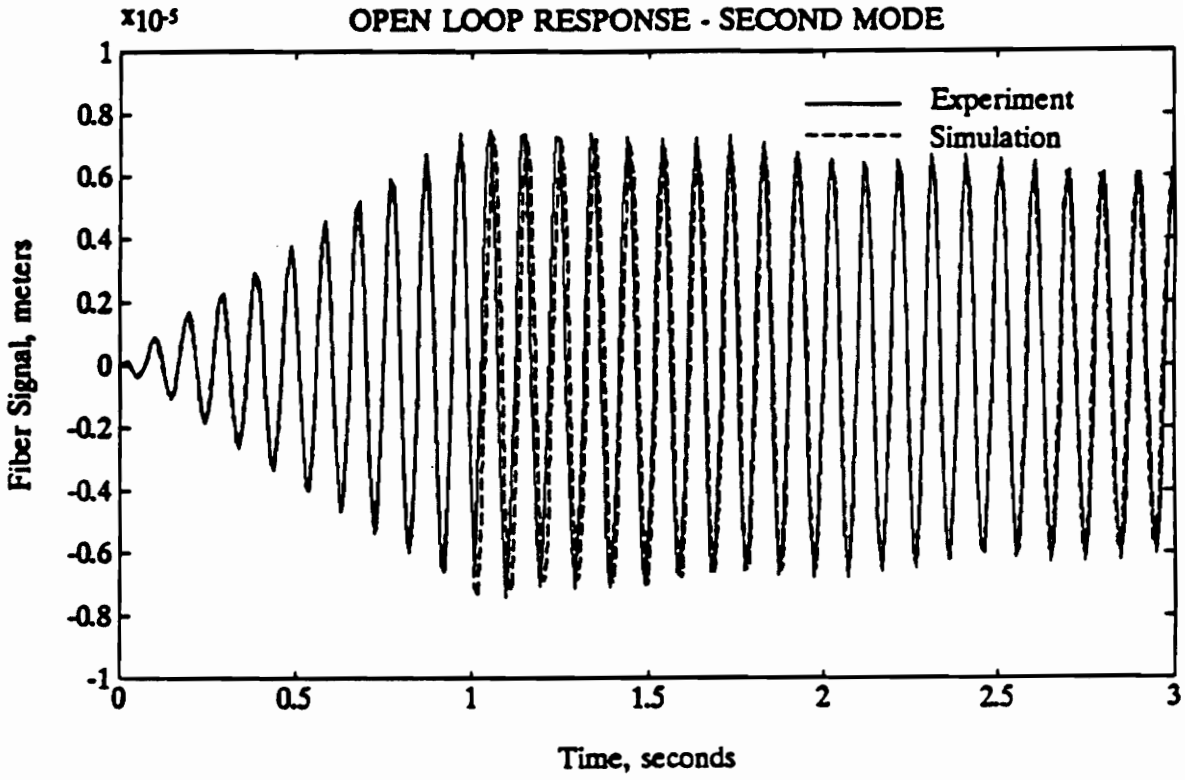

Figure 21. Simulated and experimental open loop response, second mode

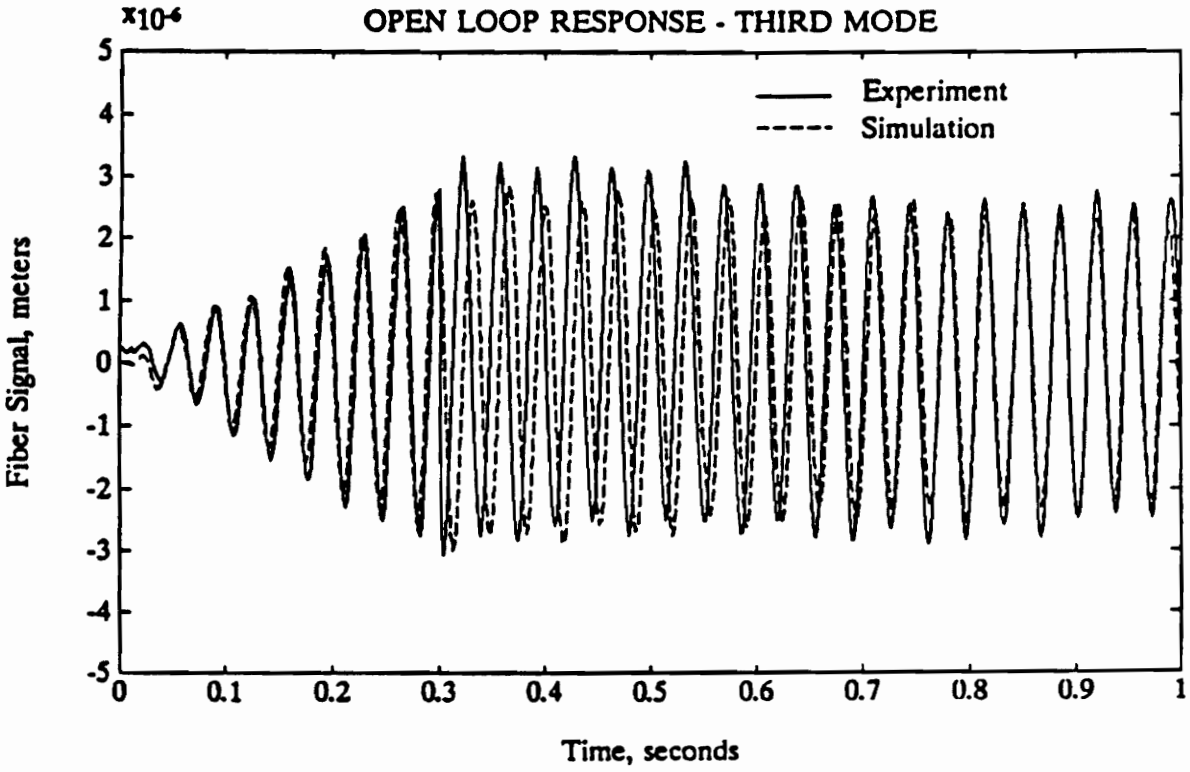

Figure 22. Simulated and experimental open loop response, third mode

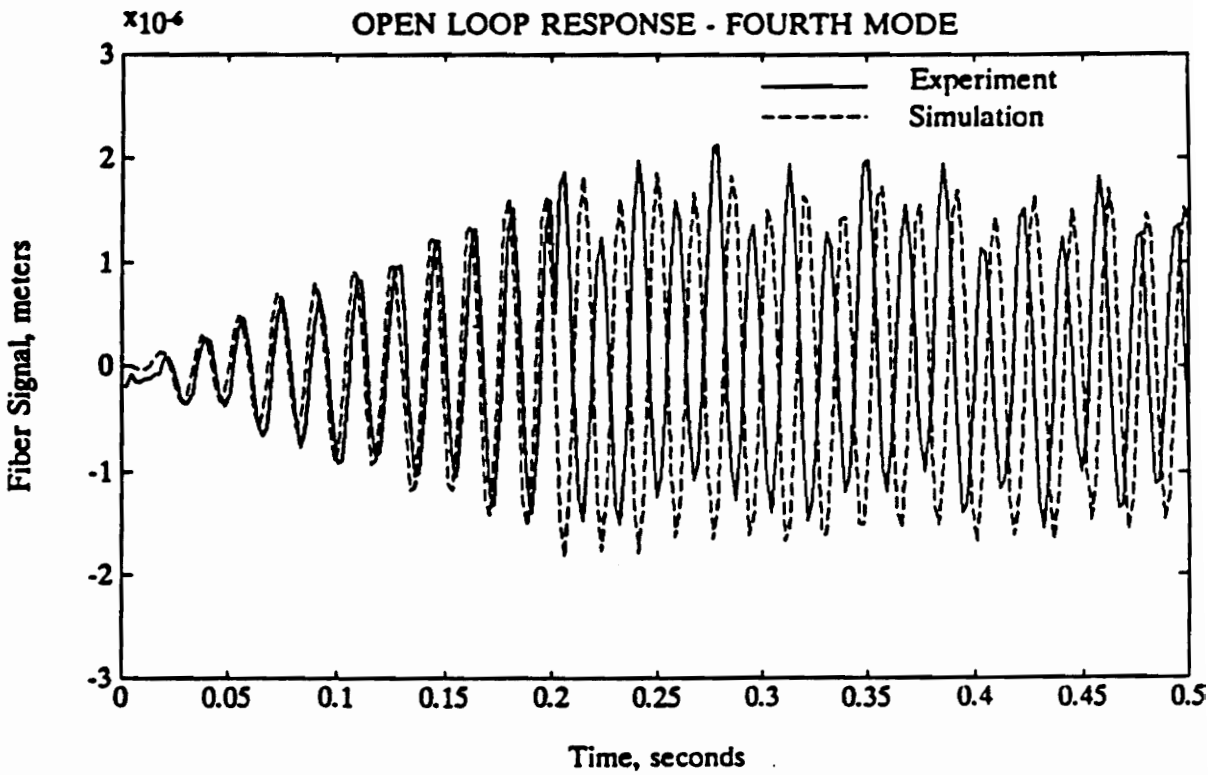

Figure 23. Simulated and experimental open loop response, fourth mode

but not in the simulation. A possible explanation lies in the fact that the piezoelectric can not only drive the beam, but also can draw energy from the beam. Strain transferred from the vibrating beam to the actuator causes a voltage to be generated across the piezoelectric. This voltage causes power to be drawn off by the low output impedance of the driving amplifier. When the driving signal is set to ground the beam receives a spike of force from the reversal of power flow. This disturbance causes a phase shift to appear in the fiber's signal.

Final verification of the dynamic system model was accomplished by comparing simulated and experimental responses to a wideband input. A variable frequency square wave was also used to excite vibrations in the beam. This input signal contained power over a broad range of frequencies, and excited many of the beam's modes. The simulated and experimental response to this input is shown in Figure 24.

5.5 CLOSED LOOP RESPONSE

The goal of this research was to demonstrate the use of a modal domain sensor in a vibration suppression control system, and to verify the modeling procedure. Since the system is linear, the response to initial vibrations in each mode is sufficient for determining the response to arbitrary disturbances. The piezoelectric actuator provided a consistent method of exciting vibrations in the beam. Therefore, in the results presented here the piezoelectric was first used to excite vibrations in the beam and then to control those vibrations. The first series of plots demonstrate the change in performance when the control system is active.

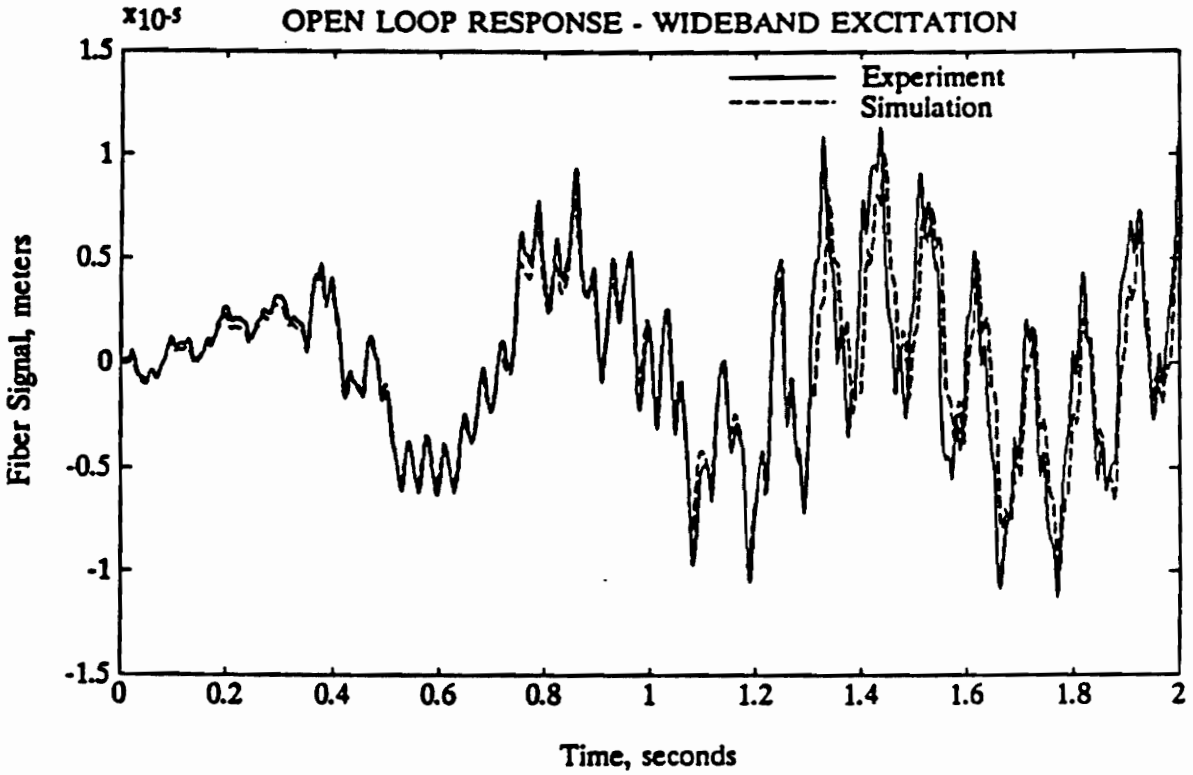

Figure 24. Simulated and experimental open loop response, wideband

These are experimental results and only the fiber's signal is shown. The second series of plots compare simulated and experimental responses. Both the signal applied to the piezoelectric and the signal received from the fiber sensor are compared.

Figures 25 thru 28 compare the open and closed loop response to modal excitation. In these plots the beam was first driven at a modal frequency then allowed to vibrate open loop for a short period of time. In the closed loop case the controller was then activated. The most damping was introduced in the first mode. The control law was designed to achieve this since first mode vibrations dominate the system's settling time. The second and third modes also experienced an increase in damping under closed loop control. The response of the fourth mode, however, appears to have the same damping in the open and closed loop configurations. At high gains the amount of damping in the fourth mode actually decreased, and stability of this mode set the limit on achievable gain. This instability is probably due to the presence of 60 Hertz line noise in the sensor's signal. The fourth mode had a frequency of 56 Hertz. When line noise was fed back through the system it caused the fourth mode to be excited. Even when the detection circuitry was run from battery power, 60 Hertz ripple was induced in the circuit. The computer's power supply was found to be creating most of the noise, however, isolating the computer was difficult and the poor performance was tolerated. The closed loop system gain was chosen low enough that the fourth mode response was not appreciably altered.

The performance of a control system depends upon the specific control law used, the sensor placement, and the authority of available actuators. No attempt

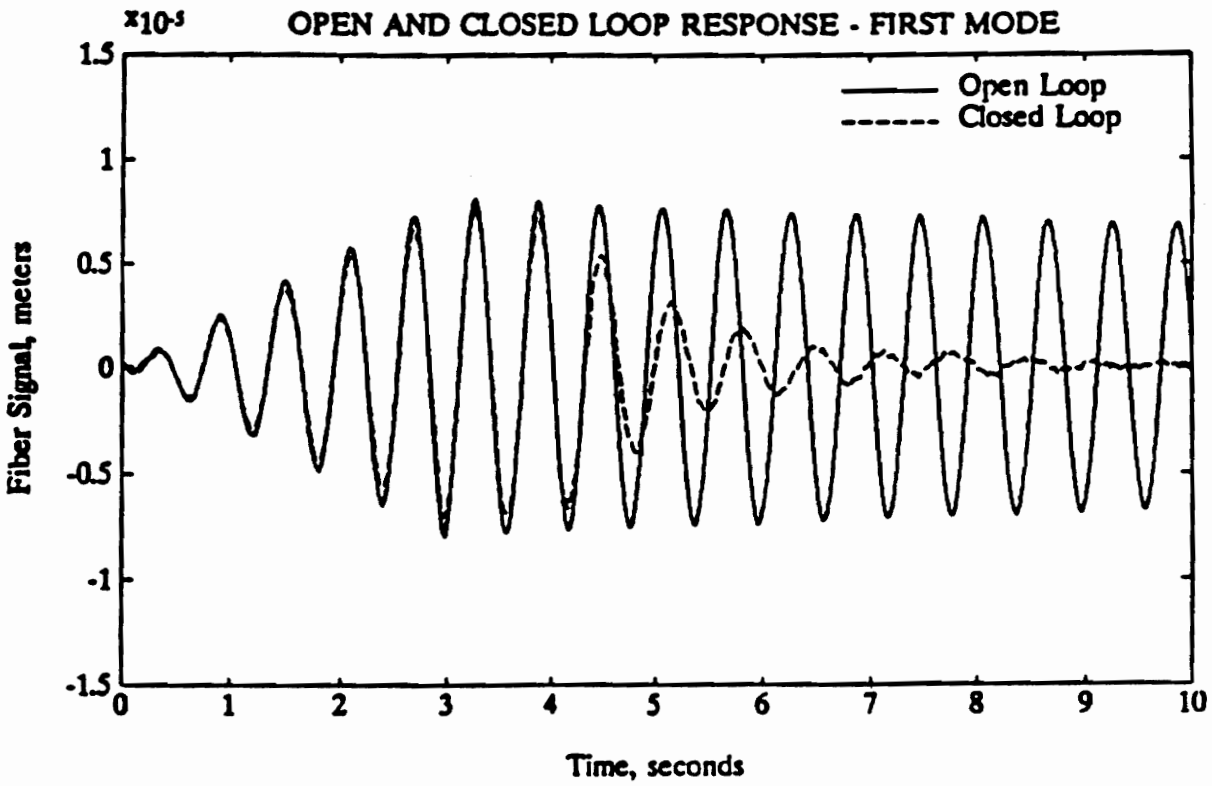

Figure 25. Experimental open and closed loop response, first mode

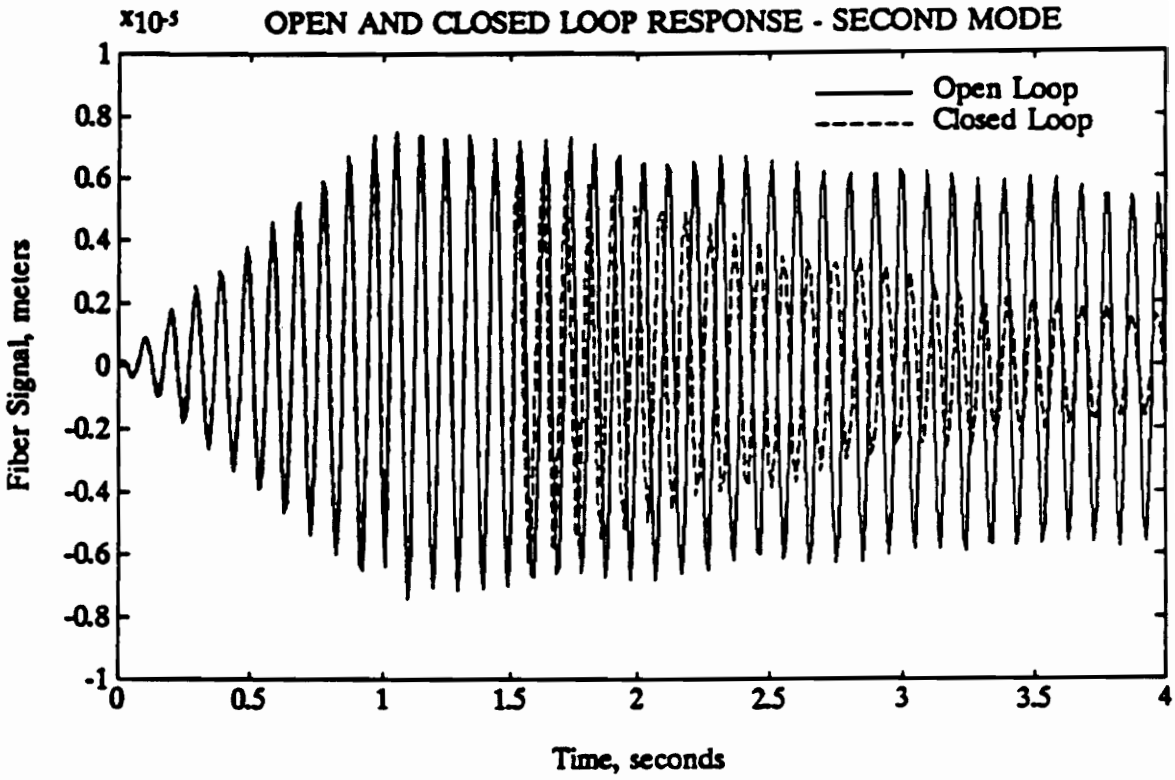

Figure 26. Experimental open and closed loop response, second mode

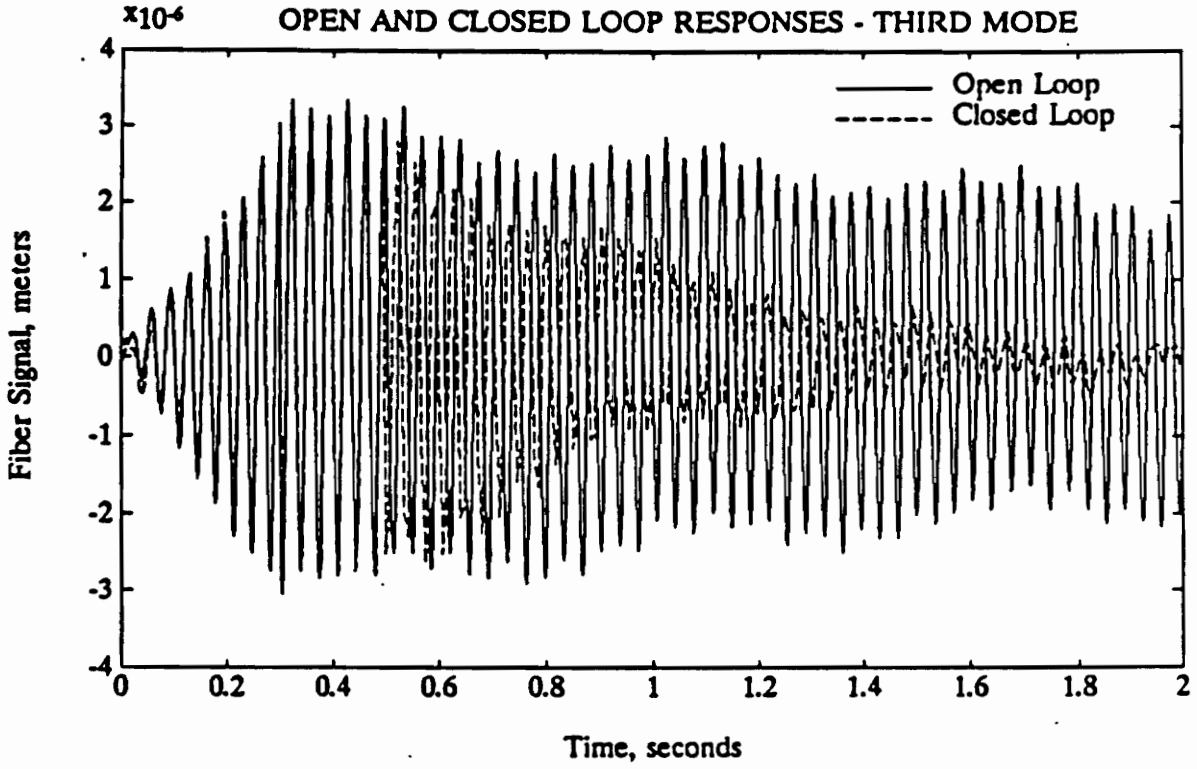

Figure 27. Experimental open and closed loop response, third mode

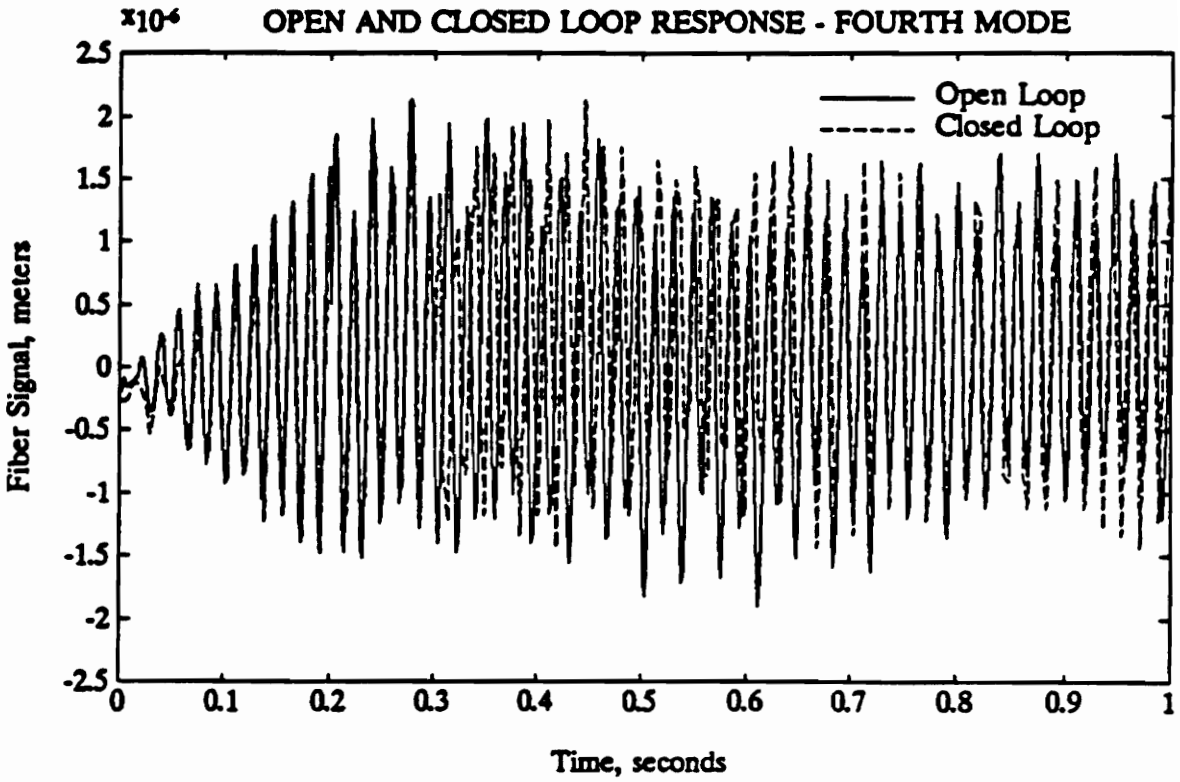

Figure 28. Experimental open and closed loop response, fourth mode

was made to optimize these factors. Instead, care was taken in modeling the system, so simulated responses would match those found experimentally. Figures 29 thru 32 compare the simulated and experimental signals for excitation in each of the first four modes. In each figure both the fiber signal, and the control signal are shown. These plots show correlation for the case of system excitation, natural response, and closed loop response. The data matches well for the first two modes. The experimental data for the third mode matches well in both amplitude and frequency. There is, however, a phase shift in the experimental data, which appears when the excitation signal is turned off. This phase shift is due to the piezoelectric actuator, driving power back into the electronics. The fourth mode signals compare in both frequency and amplitude to the simulations. The damping however is lower in the simulations. The 60 Hertz line noise apparent in the experiment was not included in the simulations. Although this discrepancy detracts from the overall system performance, it does not indicate a modeling error in either the dynamics of the system, or the response of the modal domain sensor.

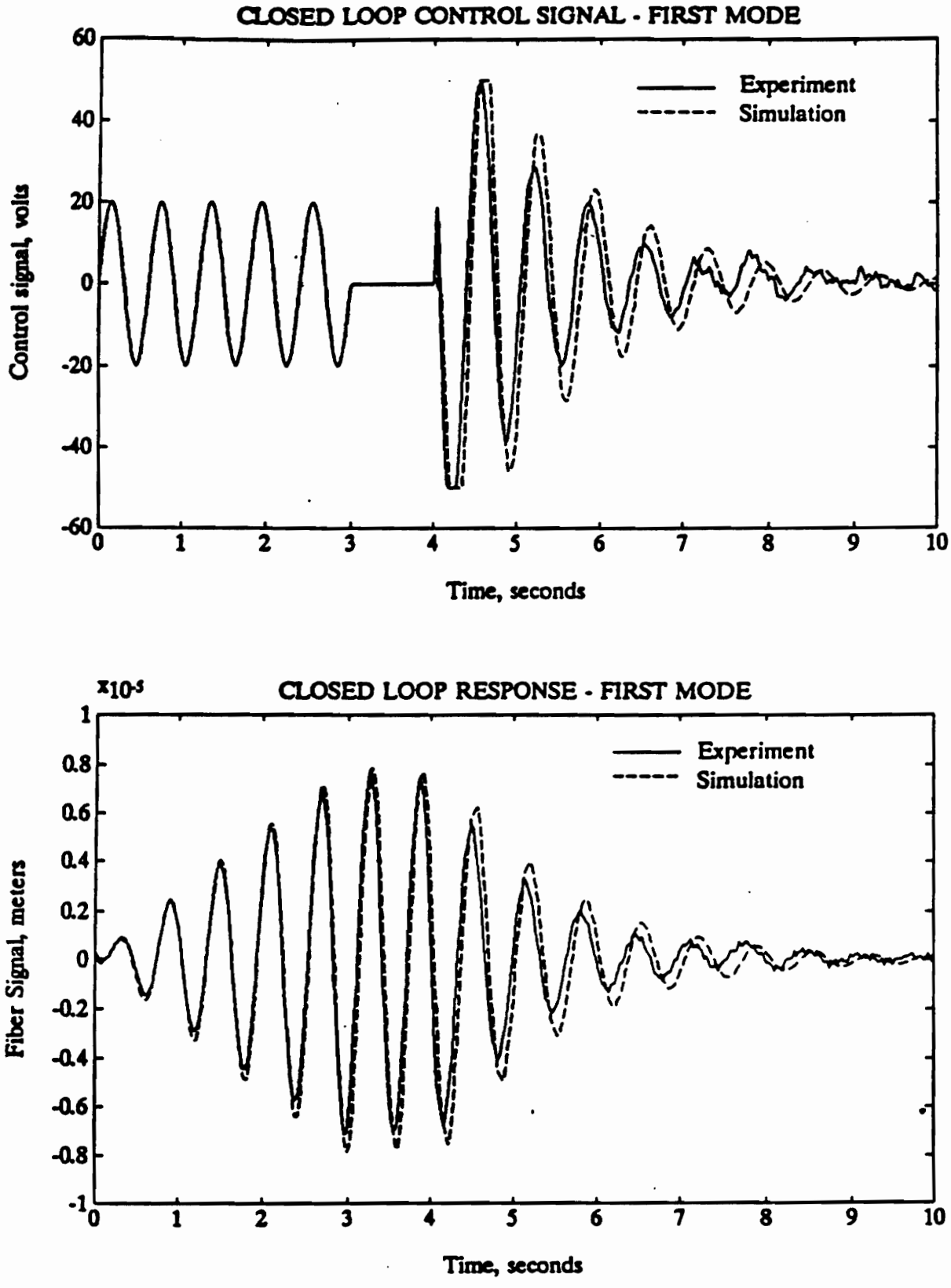

Figure 29. Simulated and experimental closed loop response, first mode

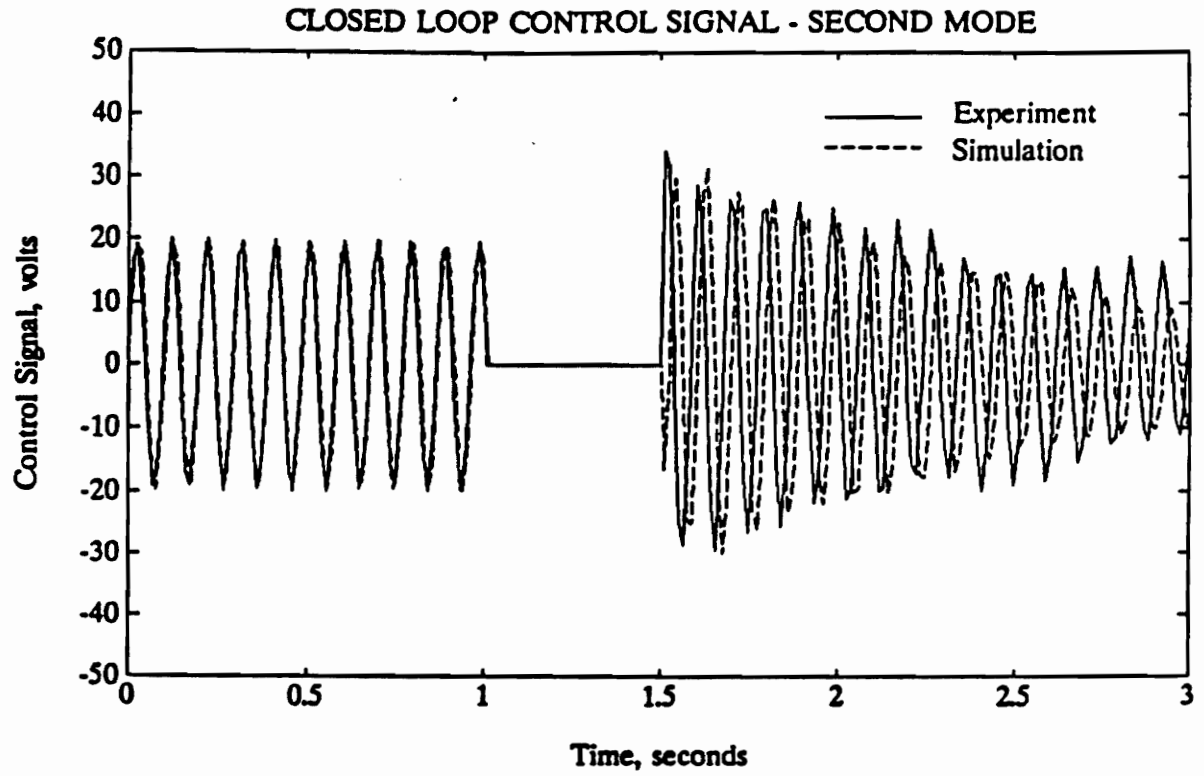

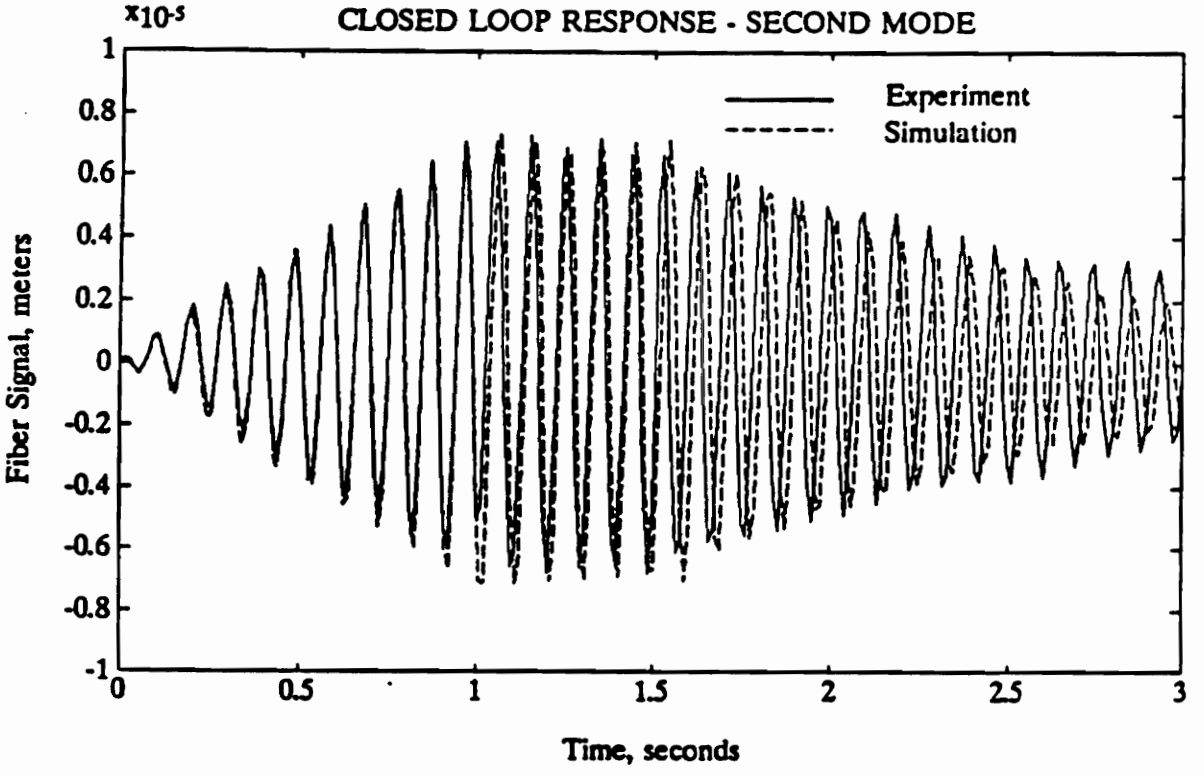

Figure 30. Simulated and experimental closed loop response, second mode

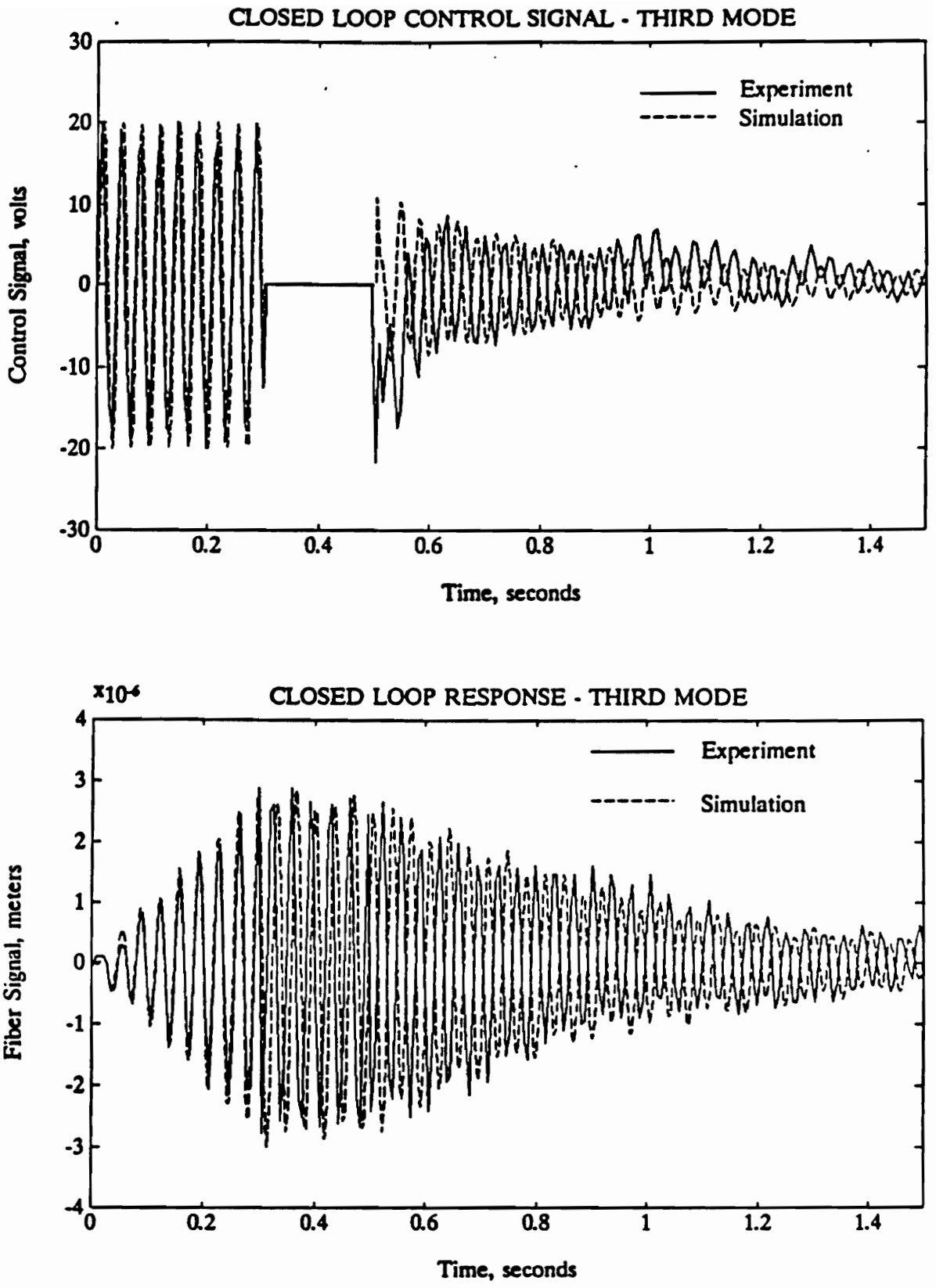

Figure 31. Simulated and experimental closed loop response, third mode

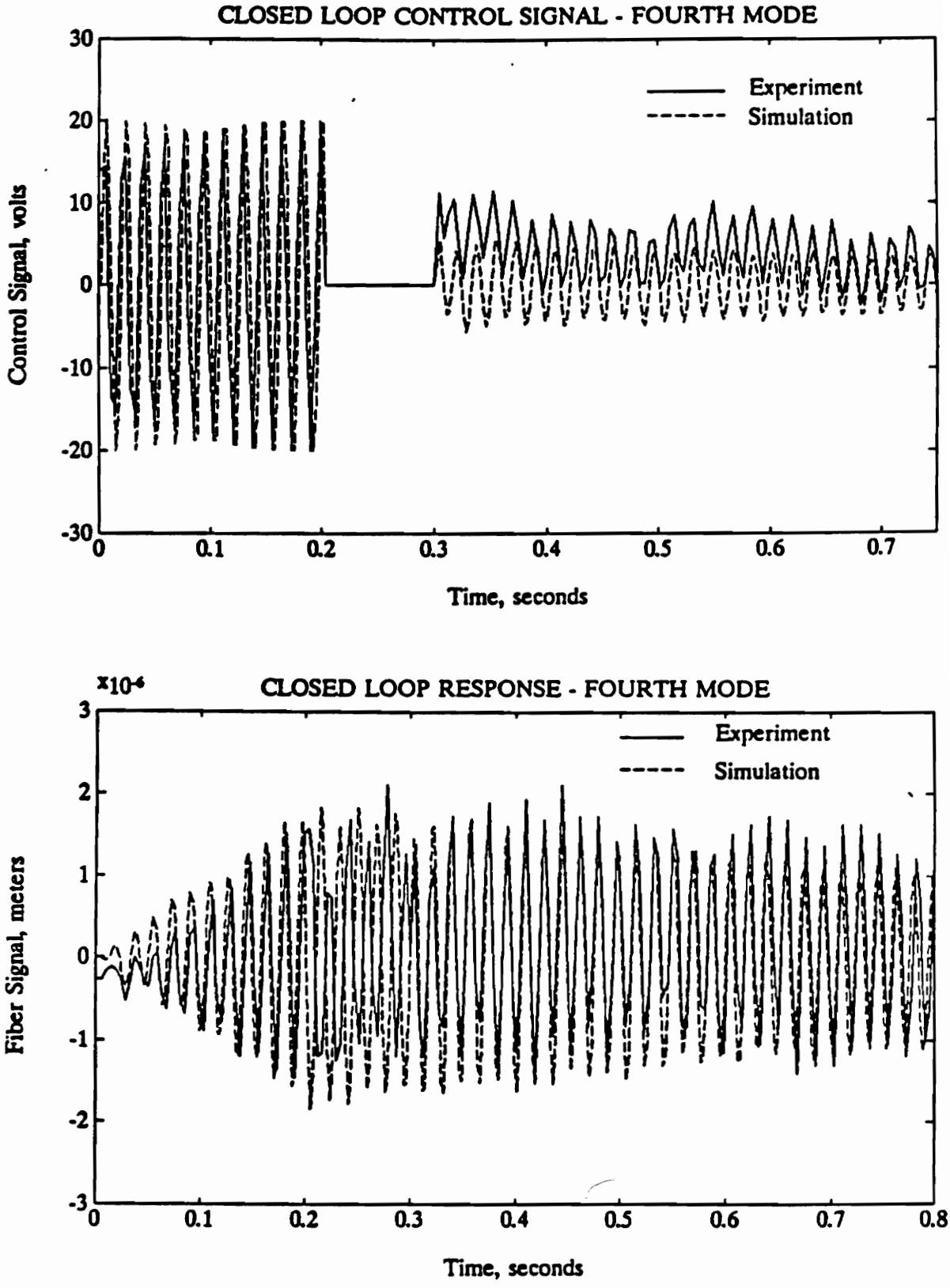

Figure 32. Simulated and experimental closed loop response, fourth mode

6.0 CONCLUSION

6.1 SUMMARY

The purpose of this research was to develop a model for the modal domain sensor, verify that model, and demonstrate the sensor in a closed loop control system. Each of these goals was accomplished. The sensor's model was developed based on the principles of circular core optical waveguides. The fiber was shown to provide a nonlinear measurement of the strain integral along its length. This model was tested by measuring both static and dynamic strain distributions. Within a linear operating range the model was shown to accurately predict the sensor's response.

A cantilevered flexible beam was instrumented with a modal domain sensor. Recent improvements in optical hardware were utilized to make the sensor robust, and immune to extraneous strains. The beam was also instrumented with a piezoelectric bending motor. A mathematical model for the flexible beam was developed. This model was combined with the sensor and actuator models to generate a representation for the system. The system model was used to design a vibration suppression control law. This control law was implemented digitally

using data acquisition boards. Dynamic tests on the first four modes of the beam verified the ability of the control law to add damping to the system.

Simulation routines were written which emulated the system, and included nonlinear effects from the sensor and actuator. The simulated system response was shown to match experimental response, under both open and closed loop conditions. The correspondence between simulations and experiment further verified the modeling procedure.

6.2 FUTURE WORK

Although this research establishes the practicality of modal domain sensing, there is still much work to be done. A full analytic description of modes in an elliptical core fiber is yet to be developed. The circular core theory proved to be an adequate approximation for this work, however, in a more sensitive application this would not be the case. The nonlinear sensor model for elliptical core fiber must account for the effect of birefringence. In order to do this the launch conditions required to excite cross polarized modes must be defined. This analysis will require accurate field descriptions of the modes.

Further research into waveguide theory could yield optical fiber designs which are tailored to sensor applications. The fibers now being used as sensors are the same as those used in communication systems. Unlike sensor applications, communication systems generally benefit from immunity to environmental disturbances. A particularly interesting design would make the fiber's sensitivity to strain vary along its length. In the sensor model this variation would appear as

a weighting function in the strain integral. This weighting function would determine the physical significance of the fiber's signal. In system applications a considerable amount of signal processing could be performed by an appropriately chosen weighting function [32].

There are also open questions in the description of strain transfer from a structure to the fiber [33]. The model developed for the modal domain sensor assumed perfect strain transfer and contained no dynamic effects. The strain transfer will be determined by method of adhering the fiber to a structure. The mounting and embedding procedures which will be used in practical systems need to be characterized. The dynamic response of the sensor will be determined by the material properties of the fiber, as well as the strain transfer from the structure. Interaction between the fiber's jacket and the cladding material has been shown to play an important role in the response of a fiber to hydrostatic pressure [34,35]. However, the affect of this interaction on the transfer of dynamic axial strains is not well known. The jacket material is typically much more pliable than the optical fiber. A detailed sensor model must account for the viscoelastic properties of the jacket, and the effect of slippage between the jacket and the cladding. Characterizing these effects could lead to jacket designs which taylor the dynamic response of the optical sensor.

APPENDIX A

This program was written to generate a state space model for the instrumented beam, from a set of physical parameters. It implements the modeling equations described in Chapter 3. It is written as a macro for the software package MATLAB. The program flow is standard, however all variables are considered matrices. All multiplication symbols imply matrix multiplications unless the variables are 1 by 1 matrices. Elements of a 1 by N matrix can be indexed by a single subscript.

```
% ***************************************************
% This program generates the state space model for a clamped free beam.
% A Modal domian sensor is assumed attached to the beam between f1 and f2.
% A piezoelectric bimorph is used as an actuator, located between p1 and p2.
%
% Requires:
%  ntop     - number of modes
%  rho      - density, mass/unit volume
%  Eb       - Young's modulus of beam
%  Ep       - Young's modulus of piezo
%  hb    - beam height
%  hp    - piezo height
%  tb       - thickness of beam
%  tp       - thickness of piezo
%  l        - beam length
%  f1,f2    - end points of fiber
%  p1,p2    - end points of piezo patch
%  d31      - piezo strain coefficent (charge constant)
%  zta      - damping factors, one for each mode (0-1)
%
% Returns:
%  A,B,C    - State space matrices
%***********************************************************
%***********************************************************
% Solutions to characteristic function
%***********************************************************
betal=[1.875104;4.694091;7.854757;10.995540;14.137168;17.27876];
betal=[betal;20.420352;23.561944;26.703537;29.845130;32.986722];
betal=[betal;36.128315;39.269908;42.411500;45.553093;48.694686];
betal=[betal;51.836278;54.977871;58.119464;61.261056;64.402649];
betal=[betal;67.544242;70.685834;73.827427;76.969020;80.110612];
betal=[betal;83.252205;86.393797;89.535390;92.676983;95.818575];
betal=[betal;98.960168;102.10176;105.24335;108.38494;111.52653];
betal=betal(1:ntop,1);
beta=betal/l;
%***********************************************************
% Initialize variables
%***********************************************************
I=1/12*hb*tb^3;
psi=(Eb*tb*hb)/(Ep*tp*hp);
cscale=1/sqrt(l);
rhol=rho*tb*hb;
m1p1=zeros(ntop,1);
m2p1=zeros(ntop,1);
m1p2=zeros(ntop,1);
m2p2=zeros(ntop,1);
m1f1=zeros(ntop,1);
m1f2=zeros(ntop,1);
Kp=zeros(ntop,1);
Q=zeros(ntop,1);
fib=zeros(ntop,1);
eps=zeros(ntop,1);
MiD=zeros(ntop,ntop);
```

```
%*********************************************************
% Generate elements of coeffiecent matrices to 2nd order diffeq system
% M*r'' + D*r'+ (Kb+Kp)*r  =  Q*v;
%*********************************************************
for i=1:ntop
  eps(i)=( cos(beta(i)*l)+cosh(beta(i)*l) )/..
                ( sin(beta(i)*l)+sinh(beta(i)*l) );

  m1p1(i)=cscale*beta(i)*( sin(beta(i)*p1) + sinh(beta(i)*p1) -..
        eps(i)*(cosh(beta(i)*p1) - cos(beta(i)*p1)) );
  m1p2(i)=cscale*beta(i)*( sin(beta(i)*p2) + sinh(beta(i)*p2) -..
        eps(i)*(cosh(beta(i)*p2) - cos(beta(i)*p2)) );

  m2p2(i)=cscale*beta(i)^2*( cos(beta(i)*p2) + cosh(beta(i)*p2) -..
            eps(i)*(sinh(beta(i)*p2) + sin(beta(i)*p2)) );
  m2p1(i)=cscale*beta(i)^2*( cos(beta(i)*p1) + cosh(beta(i)*p1) -..
            eps(i)*(sinh(beta(i)*p1) + sin(beta(i)*p1)) );

  m1f1(i)=cscale*beta(i)*( sin(beta(i)*f1) + sinh(beta(i)*f1) -..
        eps(i)*(cosh(beta(i)*f1) - cos(beta(i)*f1)) );
  m1f2(i)=cscale*beta(i)*( sin(beta(i)*f2) + sinh(beta(i)*f2) -..
        eps(i)*(cosh(beta(i)*f2) - cos(beta(i)*f2)) );

  fib(i)=tb/2*(m1f2(i)-m1f1(i));
  Kp(i)=Eb*tb^3*hp/(2*l^2*(6+psi))*( m2p2(i)*m1p2(i)-m2p1(i)*m1p1(i) );
  Q(i)= Eb*tb^2*hp*d31 / ((6+psi)*tp) * (m1p2(i)-m1p1(i));
end
M=rhol*l*eye(ntop);
Mi=inv(M);
K=Eb*I*l*(diag(beta.^4,0) + diag(Kp,0));
MiK=Mi*K;
for i=1:ntop
 MiD(i,i)=2*zta(i)*sqrt(MiK(i,i));
end
%*********************************************************
% Convert to first order diffeq system x'=Ax+Bu y=Cx  with x=[r;r']
%*********************************************************
A=[zeros(ntop,ntop) eye(ntop);-MiK -MiD];
B=[zeros(ntop,1);Mi*Q];
C=[fib'zeros(1,ntop)];

clear beta,clear m1p2,clear m2p2,clear m1p1,clear m2p1,clear fib,clear eps
clear M,clear K,clear Kp,clear Q,clear i,clear I,clear psi,clear betal
clear rhol,clear MiD,clear Mi,clear MiK,clear cscale
```

APPENDIX B

The simulation code on the following pages was used to simulate the dynamic response of the beam under open and closed loop configurations. It was compiled using Microsoft FORTRAN 4.1, and run on an IBM PS/2 Model 50. The differential equations are solved using an adaptive step routine based on the Runge-Kutta method of numerical integration. The subroutine is called DIFSOL and was written by Kenneth Becker. It is similar in design to the IMSL routine DIVPRK.

The system dynamics were based on the state space model developed in Chapter 3. However, the output of that model was warped by a sinusoid nonlinearity. This reflected the sinusoidal term in the sensor's output. The nonlinear signal was then passed through a second system of differential equations. These equations modeled the effect of the signal processing circuitry which was applied to the fiber's signal. At appropriate sample intervals the control law was evaluated using difference equations. In between sample intervals the input to the continuous system was held constant. The control signal was amplitude limited in the simulation, at the same level as in the experiment.

```
************************************************************
        PARAMETERS FOR SIMULATION  -  FILE SETUP.DAT
************************************************************
8               State space order
1               Number of sensors,rows in the c matrix
50.0            Saturation voltage
.000102         Fringe length, fiber calibration
1.0             Maximum nonlinear fiber voltage at A/D board
1.0             Simulation tolerance
0.00219         Sample time
800             Number of points saved <1000
0.0             Simulation start time
10.0            Simulation stop time
3.0             Control start time
10.0            Control stop time
0.0             Excitation start time
2.0             Excitation stop time
0               Excitation type 0-Sinusoidal,1-Data file
varsqr.dat      Datafile for excitation
20.0            Excitation Amplitude, Volts
1.67            Excitation frequency, Hertz
************************************************************
                INITIAL CONDITIONS
************************************************************
0. 0. 0. 0. 0. 0. 0. 0. 0. 0.0022
```

```
PROGRAM PIZBEAM
C*********************************************************
C DEFINE VARIABLE TYPES
C*********************************************************
      DOUBLE PRECISION X(12),XPRIME(12),NULL,WKAREA(12,12)
      DOUBLE PRECISION FIBER(5001),PIEZO(5001),TIME(5001)
      DOUBLE PRECISION TK,TKEND,TSTEP,HMIN,HMAX,HSTART,TOLER,U
      INTEGER MSIZE,IERR,NPOINTS,CROW,IPICK,UFLAG
      INTEGER NSKIP,EXTYPE,CTRIP,LSTORE,NUMOUT
      REAL A(12,12),B(12),C(12,12),Y(12),AF(4,4),BF(4),CF(4)
      REAL EXON,EXOFF,EXFREQ,EXMAG,CONON,CONOFF,VMAX,FLEN,FMAX,PICK
      CHARACTER*12 READFILE,WRITEFILE
      CHARACTER*3 NAME
      COMMON U,A,B,C,AF,BF,CF,FLEN,FMAX
      EXTERNAL XDOT
      OPEN(1,FILE='SETUP.DAT')
C*********************************************************
C READ IN DATA FROM SETUP.DAT FILE
C*********************************************************
      READ(1,*)
      READ(1,*)
      READ(1,*)
      READ(1,*)MSIZE
      READ(1,*)CROW
      READ(1,*)VMAX
      READ(1,*)FLEN
      READ(1,*)FMAX
      READ(1,*)TOLER
      READ(1,*)TSTEP
      READ(1,*)NUMOUT
      READ(1,*)TO
      READ(1,*)TF
      READ(1,*)CONON
      READ(1,*)CONOFF
      READ(1,*)EXON
      READ(1,*)EXOFF
      READ(1,*)EXTYPE
      READ(1,1010)READFILE
      READ(1,*)EXMAG
      READ(1,*)EXFREQ
      READ(1,*)
      READ(1,*)
      READ(1,*)
      READ(1,*)(X(I),I=1,MSIZE+2)
 1010 FORMAT(A)
C*********************************************************
C DEFINE INPUT AND OUTPUT FILES
C*********************************************************
      OPEN(2,FILE='MODEL.DAT')
      OPEN(4,FILE='OUTSIM.MAT',FORM='BINARY')
      OPEN(5,FILE=READFILE)
C*********************************************************
C READ IN FROM MODEL.DAT
```

```
C*********************************************************
      READ(2,*)
      DO 30 J=1,MSIZE
        READ(2,*)(A(J,K),K=1,MSIZE)
 30   CONTINUE
      READ(2,*)
      READ(2,*)(B(I),I=1,MSIZE)
      READ(2,*)
      DO 40 J=1,CROW
        READ(2,*)(C(J,K),K = 1,MSIZE)
 40   CONTINUE
      READ(2,*)
      DO 31 J=1,2
        READ(2,*)(AF(J,K),K=1,2)
 31   CONTINUE
      READ(2,*)
      READ(2,*)(BF(I),I=1,2)
      READ(2,*)
      READ(2,*)(CF(I),I=1,2)
C*********************************************************
C INITIALIZE VARIABLES
C*********************************************************
      PI = 3.14159
      YNL=0.
      CTRIP=0
      LSTORE=0
      UFLAG=0
      EXFREQ=EXFREQ*2.0*PI
      NPOINTS = NINT((TF-TO)/TSTEP)
      NSKIP=INT(NPOINTS/NUMOUT)
      IF (NSKIP.EQ.0) NSKIP=1
      NUMOUT=INT(NPOINTS/NSKIP)
      HSTART=TSTEP/10.0D0
      HMAX=TSTEP/2.0D0
      HMIN=TOL*TSTEP/10.0**2
C*********************************************************
C STEP SYSTEM THROUGH TIME
C*********************************************************
      TKEND = TO
      DO 100 K = 1,NPOINTS
        U=0.0D0
        TK = TKEND
        TKEND = TK+TSTEP
        IF (TK.GT.EXON.AND.TK.LT.EXOFF) CALL EXCIT(TK,EXFREQ,EXMAG,
     $                                    EXTYPE)
        IF (TK.GT.CONON.AND.TK.LT.CONOFF) CALL CONTROL(YNL,VMAX,CTRIP)
        CALL DIFSOL(MSIZE+2,XDOT,TK,X,TKEND,TOLER,HSTART,HMIN,HMAX,
     $             WKAREA,12,IERR)
        IF (IERR.NE.0) GOTO 999
        YNL=0.0
        DO 150 I=1,2
          YNL=YNL+CF(I)*X(MSIZE+I)
 150    CONTINUE
```

```
C*********************************************************
C SELECT POINTS FOR STORAGE
C*********************************************************
      PICK = FLOAT(K)/FLOAT(NSKIP)
      IPICK = INT(PICK)
      IF(FLOAT(IPICK).EQ.PICK) THEN
         WRITE(*,*)'PRECENTAGE OF JOB COMPLETED ',100.*K/NPOINTS
         LSTORE=LSTORE+1
         TIME(LSTORE)=TKEND
         FIBER(LSTORE)=YNL
         PIEZO(LSTORE)=U
      ENDIF
 100  CONTINUE
C*********************************************************
C STORE RESULTS IN MATLAB FORMAT
C*********************************************************
     NAME='ts'
     CALL SAVEMAT(0,NUMOUT,1,0,3,NAME,TIME,0.0D0,4,IERR)
     NAME='fs'
     CALL SAVEMAT(0,NUMOUT,1,0,3,NAME,FIBER,0.0D0,4,IERR)
     NAME='ps'
     CALL SAVEMAT(0,NUMOUT,1,0,3,NAME,PIEZO,0.0D0,4,IERR)
     CLOSE(7)
 1030 FORMAT(A)
     STOP
C*********************************************************
C ERROR HANDLING
C*********************************************************
 999  WRITE(*,*)' ERROR IN CALL IERR='
     WRITE(*,*)IERR
     STOP
     END
C*********************************************************
C----------------SUBROUTINE ----------------
C--------------------XDOT----------------------
C*********************************************************
     SUBROUTINE XDOT(SSIZE,T,X,XPRIME)
     INTEGER SSIZE,MSIZE
     DOUBLE PRECISION X(12),XPRIME(12),U,T
     REAL A(12,12),B(12),C(12,12),AF(4,4),BF(4),CF(4)
     REAL PI,FLEN,FMAX,OFFSET,INTEN
     COMMON U,A,B,C,AF,BF,CF,FLEN,FMAX
C ASSUMES SECOND ORDER FILTER
C ASSUMES FOLLOWING CONSTANTS
     PI=3.1415297
     OFFSET=1.0
     MSIZE=SSIZE-2
     DO 100 J = 1,MSIZE
       XPRIME(J) = 0.0D0
       DO 200 L = 1,MSIZE
         XPRIME(J) = XPRIME(J) + A(J,L)*X(L)
 200    CONTINUE
       XPRIME(J) = XPRIME(J) + B(J)*U
```

```
100  CONTINUE
     DL = 0.
     DO 250 J = 1,MSIZE
       DL = DL + C(1,J)*X(J)
250  CONTINUE
     INTEN=FMAX*SIN(2*PI/FLEN*DL)+OFFSET
     DO 300 J=1,2
       XPRIME(J+MSIZE)=0.0d0
       DO 400 L=1,2
         XPRIME(J+MSIZE)=XPRIME(J+MSIZE)+AF(J,L)*X(L+MSIZE)
400    CONTINUE
       XPRIME(J+MSIZE)=XPRIME(J+MSIZE)+BF(J)*INTEN
300  CONTINUE
     RETURN
     END
C*************************************************************
C--------------------SUBROUTINE-----------------------
C---------------------EXCITE-------------------------
C*************************************************************
     SUBROUTINE EXCIT(TK,EXFREQ,EXMAG,EXTYPE)
     DOUBLE PRECISION U,TK
     REAL EXMAG,EXFREQ
     INTEGER EXTYPE
     COMMON U
C*************************************************************
C DEFINE REFERENCE INPUT
C*************************************************************
     IF (EXTYPE.EQ.0) THEN
      U=EXMAG*SIN(EXFREQ*TK)
     ELSE
     READ(5,*)U
     ENDIF
     RETURN
     END
C*************************************************************
C--------------------SUBROUTINE ----------------------
C---------------------CONTROL-------------------------
C*************************************************************
     SUBROUTINE CONTROL(YNL,VMAX,CTRIP)
     DOUBLE PRECISION U
     REAL AC(12),BC(12),KCOMP,VMAX,UOLD(12),YOLD(12),YNL,TMP
     INTEGER COMPORDER,CTRIP
     COMMON U
     IF(CTRIP.EQ.0) THEN
       OPEN(3,FILE='COMP.DAT')
       READ(3,*)
       READ(3,*)
       READ(3,*)
       READ(3,*)COMPORDER
       READ(3,*)KCOMP
       READ(3,*)
       READ(3,*)(AC(J),J=1,COMPORDER+1)
       READ(3,*)
```

```
      READ(3,*)(BC(J),J=1,COMPORDER+1)
      DO 100,I=1,COMPORDER+1
        UOLD(I)=0.0
        YOLD(I)=0.0
100    CONTINUE
      CTRIP=1
    ENDIF
C*********************************************************
C EVALUATE CONTROL LAW   UOLD(1),YOLD(1) ARE PRESENT SAMPLES
C*********************************************************
    UOLD(1)=0.0
    YOLD(1)=YNL
    DO 200 I=1,COMPORDER+1
      UOLD(1)=UOLD(1)+AC(I)*YOLD(I)
200  CONTINUE
    UOLD(1)=KCOMP*UOLD(1)
    DO 300 I=2,COMPORDER+1
      UOLD(1)=UOLD(1)-BC(I)*UOLD(I)
300  CONTINUE
    UOLD(1)=UOLD(1)/BC(1)
    U=U-UOLD(1)
C*********************************************************
C CONTROL VOLTAGE SATURATION
C*********************************************************
    IF (U.GT.VMAX) U=VMAX
    IF (U.LT.-VMAX) U=-VMAX
C*********************************************************
C PERFORM SWAP ON OLD VALUES
C*********************************************************
    DO 400 I=COMPORDER+1,2,-1
      UOLD(I)=UOLD(I-1)
      YOLD(I)=YOLD(I-1)
400  CONTINUE
    RETURN
    END
C*********************************************************
C-------------------SUBROUTINE-----------------------
C-------------------- SAVEMAT-----------------------
C  AUTHOR: S.N. BANGERT 5-31-85
C  DOCUMENTATION AVAILABLE WITH MATLAB SOFTWARE
C*********************************************************
    SUBROUTINE SAVEMAT( TYPE, MROWS, NCOLS, IMAGF, NAMLEN, NAME,
   $                RPART, IPART, LUNIT, WTFLG )
        INTEGER  TYPE, MROWS, NCOLS, IMAGF, NAMLEN
        CHARACTER  NAME(*)*1
        DOUBLE PRECISION  RPART(*), IPART(*)
        INTEGER LUNIT
        INTEGER  WTFLG
        INTEGER*1  ZEROBYTE
        DATA ZEROBYTE / 0 /
        MN =MROWS*NCOLS
        WRITE(LUNIT,ERR=999)  TYPE,MROWS,NCOLS,IMAGF,NAMLEN
        WRITE(LUNIT,ERR=999)  (NAME(I),I=1,NAMLEN-1),ZEROBYTE
```

```
      WRITE(LUNIT,ERR=999)  (RPART(I),I=1,MN)
      IF (IMAGF .EQ. 1)  WRITE(LUNIT,ERR=999)  (IPART(I),I=1,MN)
      WTFLG = 0
      RETURN
999   WTFLG = -1
      RETURN
      END
```

APPENDIX C

The code given on the following pages was used to run the flexible beam experiment. It was compiled using Microsoft FORTRAN 4.1, and run on a IBM PS/2 Model 50. The software operated the data acquisition board DT2901, produced by Data Translation. Many of the subroutines called are not included in the code, but were linked in from software libraries. These libraries are part of a software package called PS/LAB, provided by Data Translation to interface with the data acquisition board.

This program allowed sinusoidal inputs, or inputs defined in data files to be applied to the piezoelectric actuator. This input data was maintained in an array as was the signal received from the fiber sensor. The program also calculated a control voltage, based on a difference equation, which could be applied to the piezoelectric actuator. Since only one sample was taken at a time the program utilized the boards programmed input output (PIO) mode of operation. To maximize the sampling rate the input-output operations were triggered from a clock pulse which greatly exceeded the achievable sampling rate. This made the actual sampling rate depend upon the speed of execution of the code. To maintain a constant rate during the 'excite', 'delay', and 'control' routines many sections of code had to be duplicated, even though the result of their execution was not needed.

```
*****************************************************************
                PARAMETER SCREEEN   -   FILE SETUP.DAT
*****************************************************************
3.0             Excitation time, seconds
1.0             Delay time, seconds
6.0             Control time, seconds, Note: 20 sec max total run
*****************************************************************
0               Excitation type 0-Sinusoid,1-From data file
input12.dat     Data file, Format - one column,voltages, -50 to 50
20.             Excitation amplitude, Volts<50
10.4            Excitation Frequency, Hertz
*****************************************************************
900             Number of points to use when storing data,<5000
*****************************************************************
0               A/D channel
0               A/D input gain (0,1,2,3),actual gain powers of 2
1               D/A channel
456.6           Board frequency, Samples per second
*****************************************************************
12.0            Gain on Compensator
4               Order of compensator
 1.0            Coefficents of numerator, decreasing powers
-3.698756
 5.404936
-3.709611
 1.005629
 1.0            Coefficents of denomenator, decreasing powers
-3.205346
 3.878054
-2.111628
 0.439881
*****************************************************************
```

```
$include:'c:\lab\pslab\lib\psldefs.for'
$include:'c:\lab\pslab\lib\pslerrs.for'
program beamprog
c*************************************************
c Declare variable types
c*************************************************
      integer*2 status,inval,outval,adhandel,dahandel
      integer*2 adbuf,dabuf,ngain,output(10000),input(10000)
      integer*2 outchannel,inchannel
      integer*4 nexcite,ndelay,ncontrol,nexamp,comporder,zero,ingain
      integer*4 i,j,nskip,narout(10000),extype,numout
      real*4 excite,delay,control,examp,exfreq,a(10),b(10),freq
      real*4 wexfreq,gain,out,arout,vmax
      double precision todisk(5000)
      character*2 name
      character*12 readfile,writefile
c*************************************************
c Read setup information
c*************************************************
      open(5,file='setup.dat')
      read(5,*)
      read(5,*)
      read(5,*)
      read(5,*)excite
      read(5,*)delay
      read(5,*)control
      read(5,*)
      read(5,*)extype
      read(5,1010)readfile
      read(5,*)examp
      read(5,*)exfreq
      read(5,*)
      read(5,*)numout
      read(5,*)
      read(5,*)inchannel
      read(5,*)ngain
      read(5,*)outchannel
      read(5,*)freq
      read(5,*)
      read(5,*)gain
      read(5,*)comporder
      do 10 i=1,comporder+1
         read(5,*)a(i)
 10   continue
      do 20 i=1,comporder+1
         read(5,*)b(i)
 20   continue
 1010 format(a)
c*************************************************
c Define constants
c*************************************************
      zero=2051
      pi=3.1415
```

```
      vmax=50.0
      ingain=2**ngain
      nexcite=nint(excite*freq)
      ndelay=nexcite+nint(delay*freq)
      ncontrol=nexcite+nint(delay*freq)+nint(control*freq)
      nskip=ncontrol/numout
      if(nskip.eq.0) nskip=1
      numout=ncontrol/nskip
      wexamp=examp/vmax*2048.
      wexfreq=exfreq*2*pi/freq
      if (extype.eq.1) then
        open(6,file=readfile)
        do 30,i=1,nexcite
          read(6,*)arout
          narout(i)=nint(arout/vmax*2047)+zero
 30     continue
      endif
C*****************************************************
c Initialize board
C*****************************************************
      adbuf=3000
      dabuf=3010
      status=psinitialize()
      status=psselectunit(1)
      status=psreset()
      status=psseterrorcontrolword(1)
      status=psdeclareuserbuffer(adbuf,2,adhandel)
      status=psdeclareuserbuffer(dabuf,2,dahandel)
      status=pslinkbuffer(0,adhandel)
      status=pslinkbuffer(1,dahandel)
      status=pssetfrequency(0,20000)
      status=pssetfrequency(1,20000)
      status=pssettransfersize(0,1)
      status=pssettransfersize(1,1)
C*****************************************************
c Excite beam
C*****************************************************
      write(*,*)
      write(*,*)
      write(*,*)'                    EXCITATION ON'
      do 100 i=1,nexcite
        status=pssetadoperation(4,1,inchannel,ngain,1,0)
        status=psdosingleoperation(0,inval)
        input(i)=inval-zero
c
        out=0.0
        do 150 j=1,comporder+1
          out=out+a(j)*float(input(i-j+1))
 150    continue
        out=out*gain
        do 175 j=2,comporder+1
          out=out-b(j)*float(output(i-j+1))
 175    continue
```

```
        outval=nint(out/b(1)+zero)
c
        outval=nint(wexamp*sin(wexfreq*float(i)))+zero
c
        if (extype.eq.1) outval=narout(i)
c
        output(i)=outval-zero
        if (outval.le.2) outval=2
        if (outval.ge.4094) outval=4094
        status=pssetdaoperation(4,outchannel,0)
        status=psdosingleoperation(1,outval)
 100  continue
c*************************************************
c Delay,  No output
c*************************************************
      write(*,*)
      write(*,*)
      write(*,*)'                    EXCITATION OFF'
      wexamp=0.
      do 200 i=nexcite+1,ndelay
        status=pssetadoperation(4,1,inchannel,ngain,1,0)
        status=psdosingleoperation(0,inval)
        input(i)=inval-zero
c
        if (extype.eq.2) outval=narout(i)
c
        out=0.0
        do 250 j=1,comporder+1
          out=out+a(j)*float(input(i-j+1))
 250     continue
        out=out*gain
        do 275 j=2,comporder+1
          out=out-b(j)*float(output(i-j+1))
 275     continue
        outval=nint(out/b(1)+zero)
c
        outval=nint(wexamp*sin(wexfreq*float(i)))+zero
c
        output(i)=outval-zero
        if (outval.le.2) outval=2
        if (outval.ge.4094) outval=4094
        status=pssetdaoperation(4,outchannel,0)
        status=psdosingleoperation(1,outval)
 200  continue
c*************************************************
c Control beam
c*************************************************
      write(*,*)
      write(*,*)
      write(*,*)'                    CONTROL ON'
      do 300 i=ndelay+1,ncontrol
        status=pssetadoperation(4,1,inchannel,ngain,1,0)
        status=psdosingleoperation(0,inval)
```

```
      input(i)=inval-zero
c
      outval=nint(wexamp*sin(wexfreq*float(i)))
c
      if (extype.eq.2) outval=narout(i)
c
      out=0.
      do 350 j=1,comporder+1
        out=out+a(j)*float(input(i-j+1))
 350   continue
      out=out*gain
      do 375 j=2,comporder+1
        out=out-b(j)*float(output(i-j+1))
 375   continue
      outval=nint(out/b(1)+zero)
c
      output(i)=outval-zero
      if (outval.le.2) outval=2
      if (outval.ge.4094) outval=4094
      status=pssetdaoperation(4,outchannel,0)
      status=psdosingleoperation(1,outval)
 300  continue
     outval=zero
     status=pssetdaoperation(4,outchannel,0)
     status=psdosingleoperation(1,outval)
     write(*,*)
     write(*,*)
     write(*,*)'                    CONTROL OFF'
c*************************************************
c Write files in MATLAB format
c*************************************************
     write(*,*)
     write(*,*)
     write(*,*)'Enter filename for data storage '
     read(*,1000)writefile
 1000 format(a)
     if (writefile.ne.' ') then
        write(*,*)
        write(*,*)
        write(*,*)'                    SAVING DATA'
        open(7,file=writefile,form='binary')
        l=0
        do 400,i=1,ncontrol,nskip
          l=l+1
          todisk(l)=float(i)/freq
 400    continue
        name='t'
        call savemat(0,numout,1,0,2,name,todisk,0.0d0,7,ierr)
        l=0
        do 500,i=1,ncontrol,nskip
          l=l+1
          todisk(l)=float(input(i))/409.6/float(ingain)
 500    continue
```

```
      name='f'
      call savemat(0,numout,1,0,2,name,todisk,0.0d0,7,ierr)
      l=0
      do 600,i=1,ncontrol,nskip
        l=l+1
        todisk(l)=float(output(i))/409.6
600    continue
      name='p'
      call savemat(0,numout,1,0,2,name,todisk,0.0d0,7,ierr)
      close(7)
      endif
      end
c**************************************************
c-------------------------SUBROUTINE-----------------------------
c------------------------- SAVEMAT--------------------------------
c  Author: S.N. Bangert 5-31-85
c  Documentation availabe with MATLAB software
c**************************************************
      subroutine savemat( type, mrows, ncols, imagf, namlen, name,
     $                    rpart, ipart, lunit, wtflg )
      integer  type, mrows, ncols, imagf, namlen
      character  name(*)*1
      double precision  rpart(*), ipart(*)
      integer lunit
      integer  wtflg
      integer*1  zerobyte
      data zerobyte / 0 /
      mn =mrows*ncols
      write(lunit,err=999)  type,mrows,ncols,imagf,namlen
      write(lunit,err=999)  (name(i),i=1,namlen-1),zerobyte
      write(lunit,err=999)  (rpart(i),i=1,mn)
      if (imagf .eq. 1)  write(lunit,err=999)  (ipart(i),i=1,mn)
      wtflg = 0
      return
999 wtflg = -1
      return
      end
```

REFERENCES

[1] T. Bailey and J. E. Hubbard, "Distributed Piezoelectric-Polymer Active Vibration Control of a Cantilever Beam," *Journal of Guidance and Control*, Vol. 8, No. 5, pp. 605-611, 1985.

[2] S. E. Burke and J. E. Hubbard, "Distributed Actuator Control Design for Flexible Beams," *Automatica*, Vol. 24, No. 5, pp. 619-627, 1988.

[3] W. Chiang and C. Lee, "Critical Active Damping Control of a Flexible Slender Plate using a Distributed Modal Actuator and Sensor," *Proceedings of the American Control Conference*, Pittsburg, PA, 1989.

[4] D. Cox, D. Thomas, K. Reichard, D. K. Lindner, and R. O. Claus, "Vibration Control of a Flexible Beam using a Distributed Fiber Optic Sensor," *Proceedings of the 28th IEEE Conference on Decision and Control*, Tampa, Florida, December 1989.

[5] D. Cox, D. Thomas, K. Reichard, D. K. Lindner, and R. O. Claus, "Modal Domain Fiber Optic Sensor for Closed Loop Vibration Control of a Flexible Beam," *Proceedings of the SPIE Symposium on Optoelectronic and Fiber Optic Devices and Applications*, Boston, Mass., September 1989.

[6] B. Culshaw, **Optical Fibre Sensing and Signal Processing**. London: Peter Peregrinus Ltd., 1984.

[7] T. Giallorenzi, J. Bucaro, A. Dandridge, G. Sigel, J. Cole, S. Rashleigh, and R. Priest, "Optical Fiber Sensor Technology," *IEEE Journal of Quantum Electronics*, Vol. QE-18, No. 4, pp. 626-665, 1982.

[8] M. R. Layton and J. A. Bucaro, "Optical Fiber Acoustic Sensor Utilizing Mode-Mode Interference," *Applied Optics*, Vol. 18, No. 5, pp. 666, March 1979.

[9] S. J. Garth, "Intermodal coupling in an optical fiber using periodic stress," *Applied Optics*, Vol. 28, No. 3, pp. 581-587, Feburary 1989.

[10] R. C. Youngquist, J. L. Brooks, and H. J. Shaw, "Two Mode Fiber Modal Coupler," *Optics Letters*, Vol. 9, pp. 177, 1984.

[11] N. K. Shankaranarayanan, *Mode-Mode Interference in Optical Fibers: Analysis and Experiment*, M.S. Thesis, Virginia Tech, March 1987.

[12] B. D. Duncan, *Modal Interference Techniques for Strain Detection in Few-Mode Optical Fibers*, M.S. Thesis, Virginia Tech, April 1988.

[13] K. D. Bennett, *Optical Fiber Modal Domain Sensors for Dynamic Strain Measurements*, PhD. Dissertation, Virginia Tech, April 1990.

[14] J. N. Blake, S. Y. Huang, B. Y. Kim, and H. J. Shaw, "Strain Effects in Highly Elliptical Core Two-Mode Fibers," *Optical Letters*, Vol. 12, pp. 732, 1987.

[15] B. Y. Kim, J. N. Blake, S. Y. Huang, and H. J. Shaw, "Use of Highly Elliptical Core Fibers for Two-Mode Fiber Devices. ," *Optical Letters*, Vol. 12, pp. 739, 1987.

[16] G. Keiser, **Optical Fiber Communications**. New York, NY: McGraw Hill Inc., 1983.

[17] D. Gloge, "Weakly Guiding Fibers," *Applied Optics*, Vol. 10. No. 10, pp. 2252-2258, 1971.

[18] A. Safaai-Jazi and R. O. Claus, "Synthesis of Interference Patterns in Few-Mode Optical Fibers," *Proceedings of the SPIE Symposium on Optoelectronic and Fiber Optic Devices and Applications*, Boston, Mass., pp. 180-185, September 1988.

[19] C. D. Butter and G. B. Hocker, "Fiber Optics Strain Gage," *Applied Optics*, Vol. 17, No. 18, pp. 2867-2869, 1978.

[20] C. Yeh, "Elliptical Dielectric Waveguides," *Journal of Applied Physics*, Vol. 33, No. 11, pp. 3235-3243, 1962.

[21] A. W. Synder and X. H. Zheng, "Optical Fibers of Arbitrary Cross Section," *Journal of Optical Society of America*, Vol. 3, No. 5 pp. 600-609, 1986.

[22] A. Kumar and R. K. Varshney, "Propagation Characteristics of Dual Mode Elliptical Core Optical Fibers," *Optics Letters*, Vol. 14, No. 15, 1989.

[23] L. Meirovitch, **Elements of Vibration Analysis**. New York, NY: McGraw-Hill Inc., 1986.

[24] J. H. Lau, "Vibration Frequencies for a Non-uniform Beam with End Mass," *Journal of Sound and Vibration*, Vol. 97, No. 3, pp. 513-521, 1984.

[25] W. T. Thomson, **Theory of Vibration with Applications**. NJ: Prentice Hall, 1981.

[26] E. F. Crawley and J. de Luis, "Use of Piezoelectric Actuators as Elements of Intelligent Structures," *AIAA Journal*, AIAA Paper 86-0878, Vol. 25, No. 10, pp. 1373-1385, 1987.

[27] E. F. Crawley and E. H. Anderson, "Detailed Models of Piezoceramic Actuation of Beams," *Journal of Intelligent Material Systems and Structures*, Vol. 1, No. 1, 1990.

[28] M. Miller, *Advances in Elliptical Core Two Mode Optical Fiber Sensors,"* MS Thesis, Virginia Tech, April 1990.

[29] D. K. Lindner, T. Celano, and E. Ide, "Vibration Suppression using a Proofmass Actuator Operating in Stroke/Force Saturation," submitted to ASME Journal of Vibrations and Acoustics, 1990.

[30] L. Ljung, **System Identificaton Theory for the User**. Prentice Hall, 1987.

[31] F. P. Beer and E. R. Johnston, **Mechanics of Materials**. New York, NY: McGraw-Hill Inc, 1981, pp.396-400.

[32] D. K. Lindner, K. M. Reichard, W. T. Baumann, and M. F. Barsky, "Measurement and Control of Flexible Structures Using Distributed Sensors," *Proceedings of the 29th Conference on Decision and Control*, December 1990.

[33] J. S. Sirkis and H. W. Haslach, "Interferometric Strain Measurement by Arbitrarily Configured, Surface Mounted, Optical Fibers," *Proceedings of the SPIE symposium on Optoelectronics, and Fiber Optic Devices*, Boston MA, 1989.

[34] B. Budiansky, D. C. Drucker, G. S. Kino, and F. R. Rice, "Pressure sensitivity of a clad optical fiber," *Applied Optics*, Vol. 18, No. 24, pp. 4085-4088, December 1979.

[35] N. Lagakos, and J. A. Bucaro, "Optimizing Polymer Coatings for Fiber Optic Acoustic Sensors," *International Wire & Cable Symposium Proceedings*, pp. 593-597, 1988.

VITA

David E. Cox was born in Elmira, New York on October 12, 1966, and graduated from Horseheads High School in 1984. He received a Bachelor of Science degree in Electrical Engineering from Virginia Polytechnic Institute and State University in May of 1988. In June of 1990 he received a Master of Science degree in Electrical Engineering, also from VPI & SU.

Mr. Cox is a member of the IEEE controls society. His professional interests include the development optical sensing techniques, and the application of control theory.